Flexible Methyl Cellulose/Polyaniline/Silver composite films with Enhanced Linear and Nonlinear Optical Properties

Ali Atta
Al Jouf University: Al-Jouf University
Mostufa Abdel Hamied
Egyptian Atomic Energy Authority
Ahmed Abdelreheem
Egyptian Atomic Energy Authority
Mohamed R. Berber (mrberber@ju.edu.sa)
Al-Jouf University College of Science https://orcid.org/0000-0002-4468-0998

Research Article

Keywords: Methyl Cellulose, Polyaniline, Silver nanoparticles, Optical properties

Posted Date: March 12th, 2021

DOI: https://doi.org/10.21203/rs.3.rs-270302/v1

Flexible Methyl Cellulose/Polyaniline/Silver composite films with Enhanced Linear and Nonlinear Optical Properties

A. Atta[1,2,], M.M.Abdelhamied[2], A.M.Abdelreheem[2], Mohamed R. Berber[3,4]

[1]*Physics Department, College of Science, Jouf University, P.O. Box: 2014, Sakaka, Saudi Arabia.*
[2]*Radiation Physics Department, National Center for Radiation Research and Technology (NCRRT), Atomic Energy Authority (AEA), Cairo, Egypt*
[3]*Chemistry Department, College of Science, Jouf University P.O. Box: 2014, Sakaka, Saudi Arabia*
[4]*Department of Chemistry, Faculty of Science, Tanta University, Tanta 31527, Egypt*

[*]*corresponding author: mberber@ju.edu.sa;* aamahmad@ju.edu.sa

Abstract

In order to potentiate implementations in optical energy applications, flexible polymer composite films comprising methyl cellulose (MC), polyaniline (PANI) and silver nanoparticles (AgNPs) were successfully fabricated through a solution cast preparation method. The composite structure of the fabricated film was confirmed by X-ray diffraction and infrared spectroscopy, indicating a successful incorporation of AgNPs into the MC/PANI blend. The optical parameters such as band gap (E_g), absorption edge (E_d), number of carbon cluster (N) and Urbach energy (E_u) of pure MC polymer, MC/PANI blend and MC/PANI/Ag film were determined by using the UV optical absorbance in the wavelength range 200 to 110 nm. The influence of AgNPs and PANI on linear optical (LO) and nonlinear optical (NLO)parameters such as reflection extinction coefficient, refractive index, dielectric constant, nonlinear refractive index and nonlinear susceptibility of MC polymer were also investigated. The results showed a decrease in the band gap of MC/PANI/AgNPs compared to the pure MC film. Meanwhile, the estimated carbon cluster number enhanced with the incorporation of the AgNPs. The addition of AgNPs and PANI also improved the optical parameters of MC polymer, a trait that makes the current composite a convenient material for optical energy applications.

Keywords: Methyl Cellulose; Polyaniline; Silver nanoparticles; Optical properties

1. Introduction:

Flexible composite materials are receiving a great deal of attention in optical energy applications due to their remarkable electrical, thermal, mechanical, dielectric and optical properties versus the other traditional materials [1-2]. Currently, polymer composites are of high interest in different energy applications because of their pliable characteristics and their easy to use. [3]. Huge attention has been given to reveal the optical properties of polymers, and to potentiate their implementations in optical energy applications [4].

Among the various polymers used in optical energy applications, is the polyaniline (PANI). PANI has been widely studied as a nonlinear optical (NLO) material because of its UV radiation resistance, ultrafast response, steady electrical conductivity, flexibility and easy relative processing [5]. However, PANI has limited mechanical properties, fusibility, and solubility. Thus, it has to be modified with other materials to improve these limitations and to enhance its uses, especially in energy applications. On the other hand, MC polymer is a semi-crystalline structure water soluble polymer carries high mechanical properties, a unique chemical stability, and a perfect optical behavior [6-7]. Hence, the composite of MC and PANI is envisioned to provide a material with remarkable optical properties.

The incorporation of inorganic fillers into the polymer matrix is of much interest, because such inorganic-polymer composites have paved the road to modify the polymer composite properties, providing additional and remarkable optical features [8-9]. Conducting-fillers such as AgNPs have showed many advantages in various applications (e.g. conductive inks, photonics and electronic chips, sensors, batteries and solar cells) because it can decrease the optical band gap [10-11]. Thus, the incorporation of AgNPs into the Mc/PANI polymer matrix is a topic of interest.

In the current study, we aim to prepare a flexible composite of AgNPs and MC/PANI polymer matrix, studying the possibility of enhancing the optical properties of MC e.g. optical band gap (E_g), band tail (E_e), absorption edge (E_d), refractive index (n), extinction coefficient (K), dielectric constant and optical conductivity. The linear/nonlinear optical parameters (extinction coefficient, refractive index, reflectance, first order linear optical susceptibility, real and imaginary dielectric constant, and third order nonlinear optical

susceptibility) of MC/PANI/AgNPs composite films will be determined by using the UV–Vis spectroscopy.

2. Materials and methods

2.1 Materials

Methyl cellulose (MC; MW 658.7 g/mol) was purchased from Sigma-Aldrich, Hydrochloric acid (35%), and Ammonium peroxidisulfate (grade, 99%), were purchased from Merck Darmstadt Germany, aniline monomer ($C_6H_5NH_2$) was purchased from Oxford Lab Chemistry, and $AgNO_3$ was purchased from Nice Chemicals PVT.

2.2 Preparation of MC/PANI/AgNPs composite film

PANI has been prepared by an oxidation polymerization process of aniline in hydrochloric acid using ammonium peroxide-sulfate as an oxidative agent [12]. For the synthesis of MC/PANI blend, 1.0 g of MC was dissolved in 50 mL distilled water at room temperature. Then, 1.0 wt% and 3.0wt% of PANI were added separately to MC solution. The resultant mixture was stirred by an ultrasonic probe at room temperature till a homogenous solution was obtained.

Regarding the preparation of MC/PANI/AgNPs composite films, $AgNO_3$ powder was added with different concentrations (0.5 wt% and 1.0 wt%) over a period of 30 min under continuous stirring to the MC/PANI composite. Then, the reducing agent $NaBH_4$ was added dropwise to the composite mixture over a period of 60 min. Subsequently, the obtained mixture was added on a petri dish to cast a film.

2.3 Characterization techniques

The structural properties of the pristine MC film, MC/PANI blend and the MC/PANI/Ag composite films were investigated by using a X-ray powder diffraction (Shimadzu XRD-6000). The chemical bonds and functional groups of prepared films are identified using FTIR spectroscopy (ATI Mattson, Genesis series, Unicam, England). The

optical properties of the prepared films were investigated by a UV–vis spectrometer (JascoV-670 UV-VIS spectrophotometer) in the wavelength range 200 nm to 1100 nm.

3. Results and Discussion

3.1 Structural investigation of the synthesized films

The XRD spectrum of pristine MC, PANI/MC blend, and Ag/PANI/MC composite films are shown in Fig.1. The spectrum of MC has indicated two diffraction peaks at 8.1° and 20.7° characteristic for MC with a partial crystalline structure. The area under the peak 8.1° of MC was 1104. The XRD pattern for MC/3%PANI film has become more amorphous with almost disappearance of the MC diffraction peak at 20.7°. The area under the peak 8.1° of MC has changed from 1104 to 4066, confirming the amorphous structure of MC obtained after the addition of PANI. This reduction of the MC crystallinity suggested a good interaction between the chains of MC and PANI polymer [13]. The XRD of MC/3%PANI/0.5%Ag has showed a new peak at 38.6° which is attributed to the (111) diffraction peak of the face-concentrated-cubic AgNPs. The expansion of full width half maximum (FWHM) of MC characteristic peak at 8.1° has proved a good diffusability of the AgNPs into the MC/PANI blend. The average crystallite size (D) of AgNPs determined from Scherrer equation [14] was 13.5 nm.

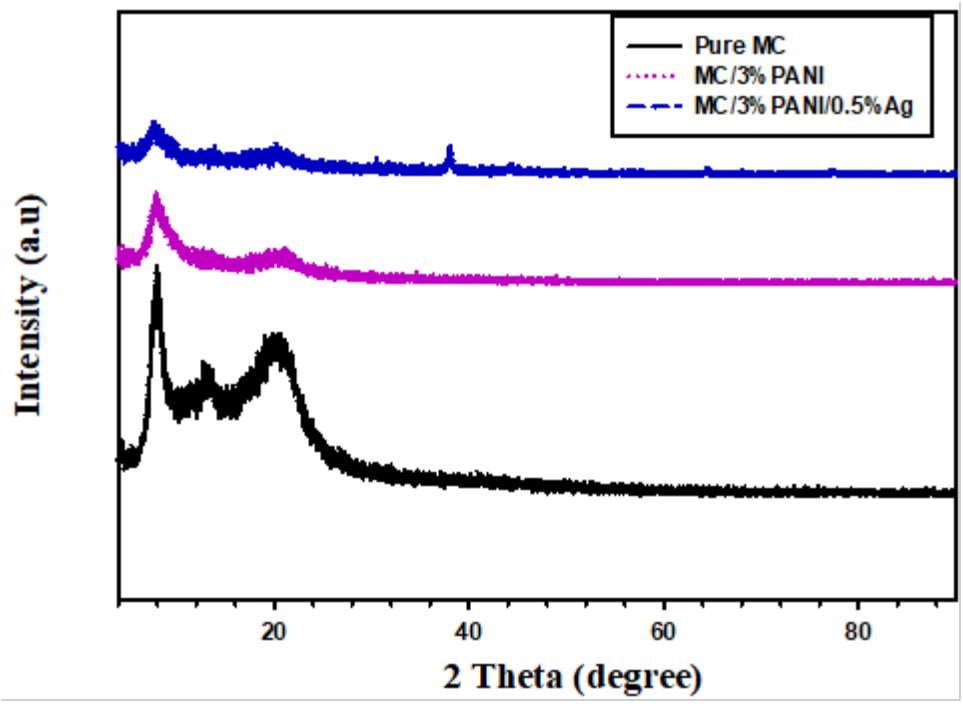

Fig.1: XRD patterns of pristine MC, MC/3%PANI and MC/3%PANI/0.5Ag films

Furthermore, the IR data displayed in Fig. 2 confirmed the structure of synthesized films. Specifically, the black IR spectrum of Fig. 2 has showed the characteristic absorption bands C-O-C stretching vibration, C-H stretching vibration, and O-H stretching vibration of MC at 1110 cm^{-1}, 2900 cm^{-1} and 3400 cm^{-1}, respectively [15]. After the addition of PANI (yellow and red spectrum), the intensity of the absorption bands of MC has lowered especially the OH stretching vibration band. This lowering of the beaks intensity suggested a breakage of the hydrogen bonding network of MC and the penetration of PANI between the chains of MC. In addition, the characteristic absorption bands of PANI, in particular, the C–N and C=N stretching vibrations have newly emerged at 1250 $cm^{-1}$and 1550 cm^{-1}, respectively [16].. The addition of AgNPs (green and blue spectra) has showed no change in the spectra of MC/PANI blends. Only, new bands characteristic for the metal particles have been observed at 750 and 820 cm^{-1} in the spectrum of the MC/PANI/AgNPs composite [17].

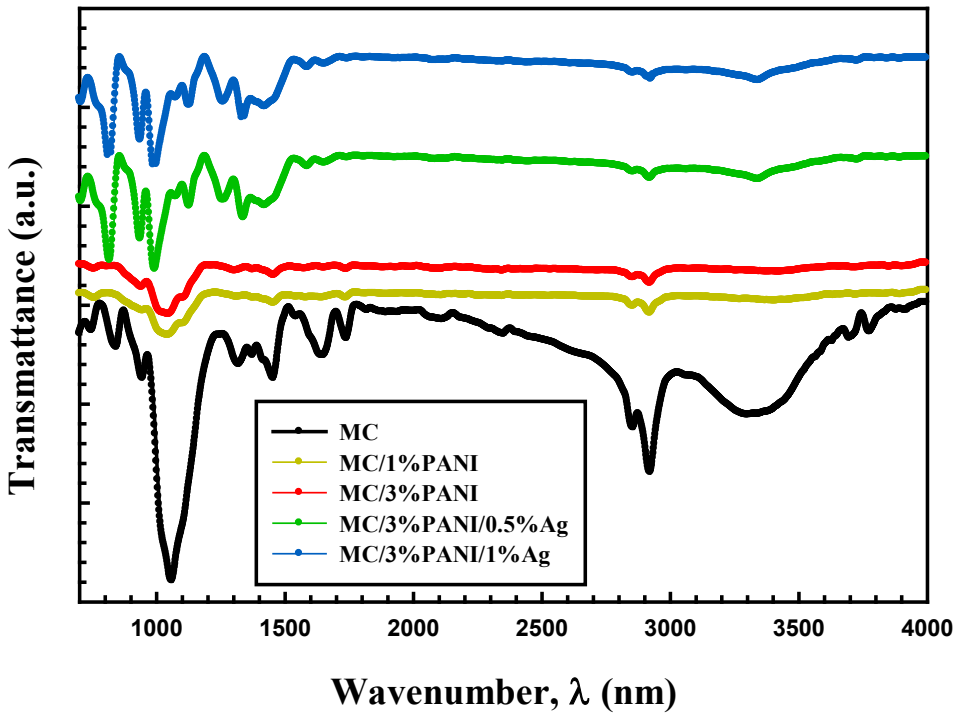

Fig2: IR spectra of pristine MC, MC/1%PANI, MC/3%PANI, MC/3%PANI/0.5%Ag and MC/3%PANI/0.5Ag films

3.2. Optical properties of the synthesized films.

The UV–vis optical absorption of pristine MC, MC/PANI and MC/PANI/Ag films are shown in Fig.3. As observed, the MC absorption peak has increased with the addition of PANI. The two peaks of MC and PANI has also overlapped as a result of the blending process [18]. After the addition of AgNPs, a new adsorption peak characteristic for the surface plasmon resonance (SPR) of the electrons of AgNPs is observed [19]. From the FWHM ($\Delta E_{1/2}$) of SPR band, the radius (r) of AgNPs has been estimated assuming free particles behaviour of conduction electrons, using equation (1) [20]:

$$r = \frac{h\,v_f}{\Delta E_{1/2}} \qquad (1)$$

Where v_f =1.39×10^6 m/s related to Fermi velocity of electrons in silver bulk and h is Planck's constant. The calculated average particle size of AgNPs was found to be 10 nm, which is close to the value calculated from XRD.

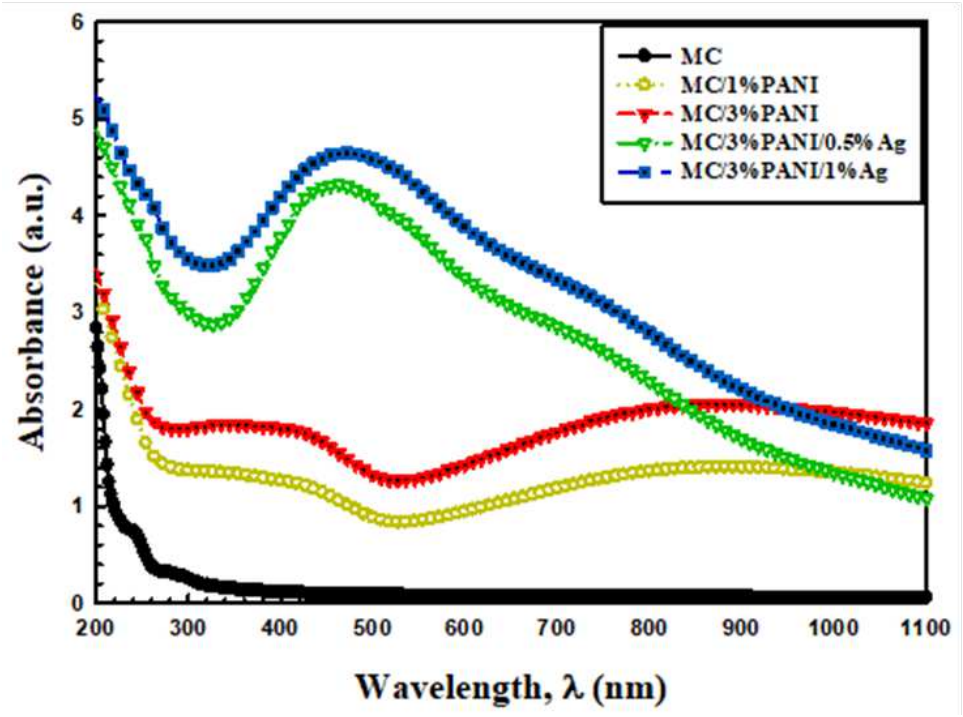

Fig.3: UV-Vis Absorption spectra of pristine MC, MC/1%PANI, MC/3%PANI, MC/3%PANI/0.5%Ag and MC/3%PANI/1%Ag films.

The absorption coefficient α (ν) is estimated using equation (2) [21].

$$\alpha(\nu) = \frac{2.303\ A}{d} \qquad (2)$$

Where, A indicates the optical absorbance and d is the film thickness. The absorption optical coefficients with photon energy of pristine MC, MC/1%PANI, MC/3%PANI, MC/3%PANI/0.5AgNPs, and MC/3%PANI/1AgNPs films are shown in Fig.4. The absorption edge (E_d) value was determined from extrapolating the linear part of α against applied hν curves at absorption zero value [22]. As shown, the absorption edge E_d decreased by the addition of AgNPs and PANI to MC polymer (see the details of Table 1). The E_d decreased from 5.42 eV for pristine MC to 3.14 eV for MC/3%PANI and reduced to 1.93 eV for MC/3%PANI/1%AgNPs. This reduction in E_d was related to the changes in the hole and

the electron numbers in the conduction and the valence bands [23]. Another factor for shifting absorption edge was the structural changes in MC polymer matrix, which has been confirmed by the XRD results and the molecular interactions of MC polymer chains and the AgNPs. In other words, the shift in the optical absorption edge has reflected the electronic conjugation between the AgNPs and the PANI beside the increase in the degree of disorder for those composite films [24].

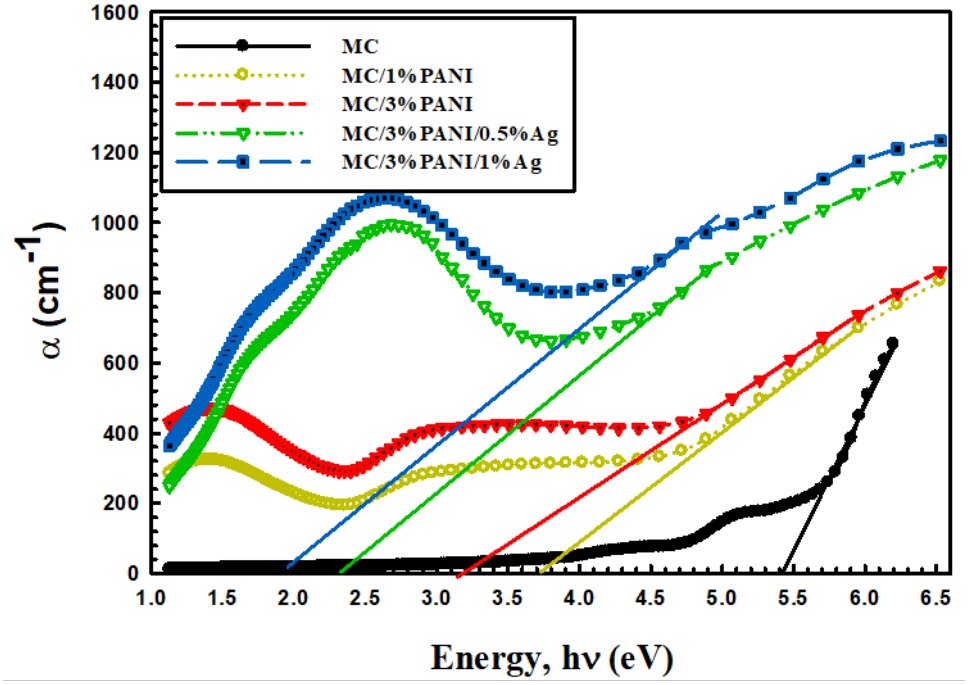

Fig.4: Absorption coefficients α as a function of wavelength for pristine MC, MC/1%PANI, MC/3%PANI, MC/3%PANI/0.5%Ag and MC/3%PANI/1%Ag films

The energy band gap (E_g) of all films have been determined from the intercept of the additional plotted linear portion $(\alpha h\nu)^2$ versus hν as shown in Fig. 5, which pursues Tauc method (equation 3)[25]:

$$\alpha h\nu = B(h\nu - E_g)^n \qquad (3)$$

where B represents the absorption edge width parameter, hν is the incident photon energy calculated from $h\nu=1240/\lambda$, and n is factor takes 3/2 or 1/2 for direct transitions and 2 or 3 for indirect transitions depending on forbidden or allowed transition respectively. The

determined values of direct E_g are listed in Table 1. As observed, E_g has decreased from 5.76 eV for pristine MC, to 5.01eV for MC/3%PANI, and reduced to reach 4.27eV for MC/3%PANI/1%AgNPs. The reduction in MC optical gap was due to the variations of polymer disorder [26]. In addition, the defects induced by the localized states in the band gap, was the main reason for reducing energy band of the polymer. Furthermore, the reduction in optical band gap was related to the charge transfer complexes (CTCs) formation due to the trap levels between LUMO and HOMO bands of MC polymer [27], which enhanced the lower transitions energy. This successfully implies the miscibility of AgNPs and MC/PANI blend chains and strongly supports the XRD results.

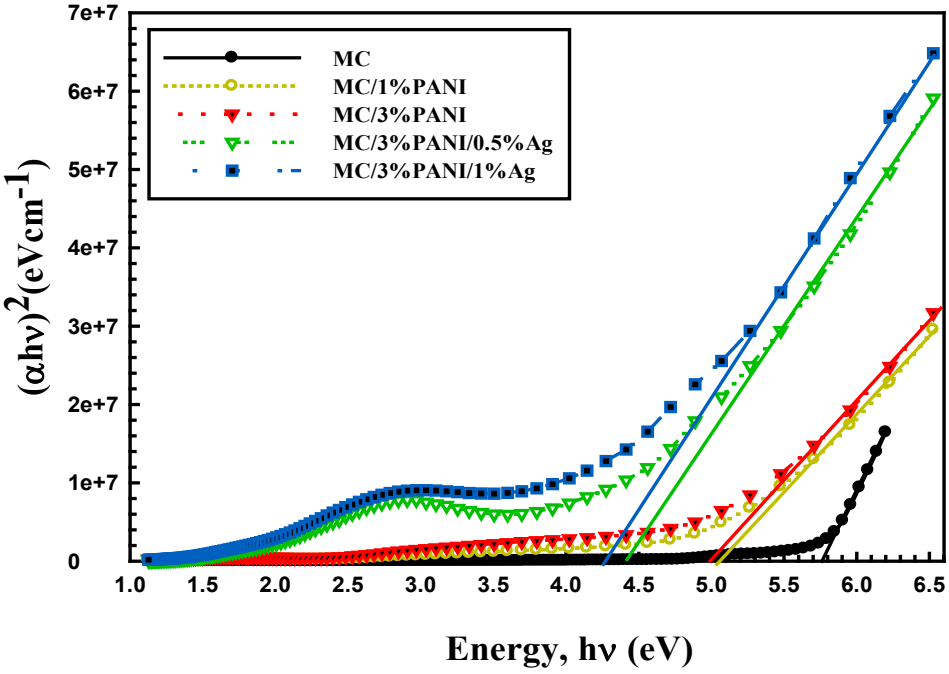

Fig.5: The relation between $(\alpha h\nu)^2$ against photon energy ($h\nu$) for pristine MC, MC/1%PANI, MC/3%PANI, MC/3%PANI/0.5%Ag and MC/3%PANI/1%Ag films.

For determining the band tail that refers to the width of localized states, the absorption coefficient α (ν) near band edge as exponential dependence of photon energy ($h\nu$) has been determined from the Urbach relationship (equation 4) [28]:

$$\alpha(\nu) = \alpha_o \, e^{\left(h\nu / E_e\right)} \qquad (4)$$

The Urbach tail E_e value recorded in Table 1, has been determined by the reciprocal of the slope of the linear portion of the curves shown in Fig.6. As observed, E_e enhanced from 0.51 eV for pristine MC to 1.52 eV for MC/3%PANI and increased to reach 2.02 eV for MC/3% PANI/1%AgNPs. The band tail E_e values has inversely changed with band gap E_g values. This was a result of the disorder induced in the MC polymer chain after the incorporation of the AgNPs that induced interaction changes in MC/PANI polymer blend [29]. In other words, the changes of Urbach tail E_e was a result of the defects in the MC chains after the addition of PANI and AgNPs. Specifically, the AgNPs and PANI has led to the redistribution from the band states, permitting additional tail to tail transitions [30].

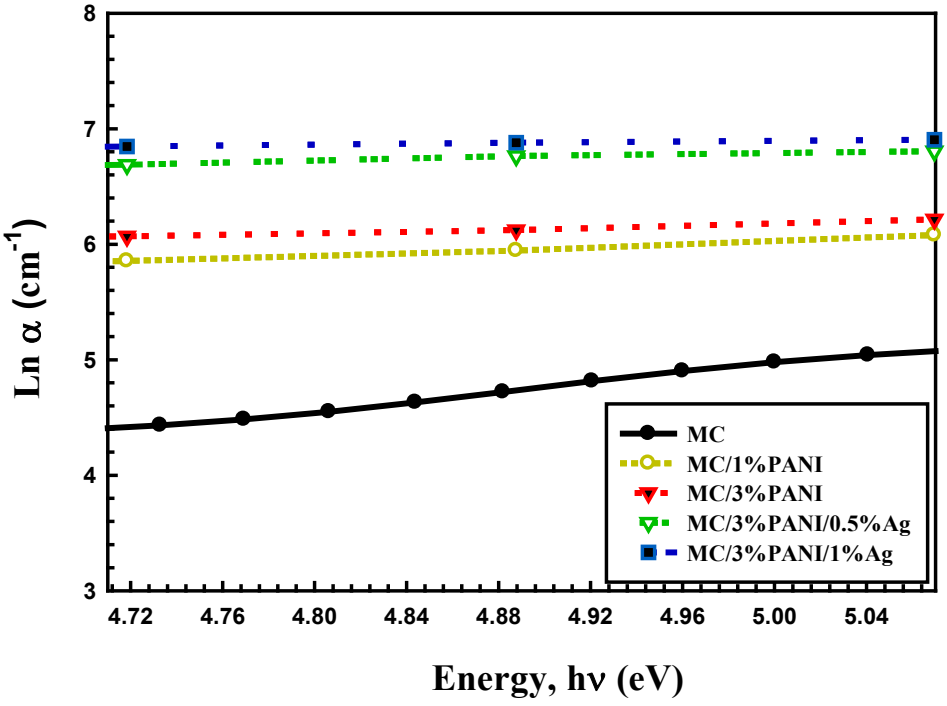

Fig.6: Absorption coefficient versus photon energy for pristine MC, MC/1%PANI, MC/3%PANI, MC/3%PANI/0.5Ag and MC/3%PANI/1%Ag films

The carbon cluster number (N) has been estimated from optical gap E_g using equation (5) [31]:

$$E_g = 34.4/\sqrt{N} \qquad (5)$$

The estimated N value (see Table 1) of pristine MC was 36. Aftet the addition of PANI, It has increase to be 47, and has increased to reach 65 for MC/3%PANI/1%AgNPs film. This enhancement of N number was a result of the conjugation of monomer units in MC polymer matrix after the addition of PANI and AgNPs in the MC polymer. The enhancement of the N values has been attributed to the amounts of the conducting PANI and the AgNPs, where the higher their content in the host MC matrix, the more defects are introduced causing additional low energy states, and hence a decrease in the band gap is observed leading to an improvement in the N value.

Table.1. Values of absorption edge E_d, band gap E_g , band tail E_e, and carbon cluster number N of pristine MC, MC/1%PANI, MC/3%PANI, MC/3%PANI/0.5%Ag and MC/3%PANI/1%Ag films

The samples	Absorption edge E_d (eV)	Optical band gap E_g (eV)	Urbach energy E_e,(eV)	Carbon cluster number (N)
Pure MC	5.42	5.76	0.51	36
MC/1%PANI	3.70	5.06	1.38	45
MC/3%PANI	3.14	5.01	1.52	47
MC/3%PANI/0.5%Ag	2.38	4.41	1.92	61
MC/3%PANI/1%Ag	1.93	4.27	2.02	65

The extinction coefficient (K), which is an indication of the debility of absorption alterations when the electromagnetic wave spreads across the material, has been calculated using equation (6) [32].

$$K = \frac{\alpha\lambda}{4\pi} \qquad (6)$$

The extinction coefficient k is plotted as a function of wavelength as shown in Fig.7. As seen, k has displayed high values at the longest wavelengths. This behavior is ascribed to the high absorption coefficient in this region. On other hand, the extinction coefficient k has enhanced by addition of PANI and AgNPs to the MC polymer chain. This is because; PANI and AgNPs have induced modification on polymer structure. Another reason for the enhanced extinction coefficient k was a result of the surface SPR of drugged AgNPs in MC polymer. Additionally, the extinction coefficient K of MC/3%PANI/0.5%AgNPs observed at λ of 490 nm has shifted to λ of 520 nm for MC/3%PANI/1%AgNPs film. This shift in

wavelength with increasing AgNPs was a result of the new levels in the optical band gap that has led to more crossing of electrons from valence to conduction band [33].

Furthermore, the higher value of the extinction coefficient of MC/PANI/1%AgNPs has showed more scattering of light compared to MC/PANI/0.5%AgNPs. This increase of the the extinction coefficient of MC/PANI/1%AgNPs was a result of the enhanced interactions of AgNPs and PANI [34].

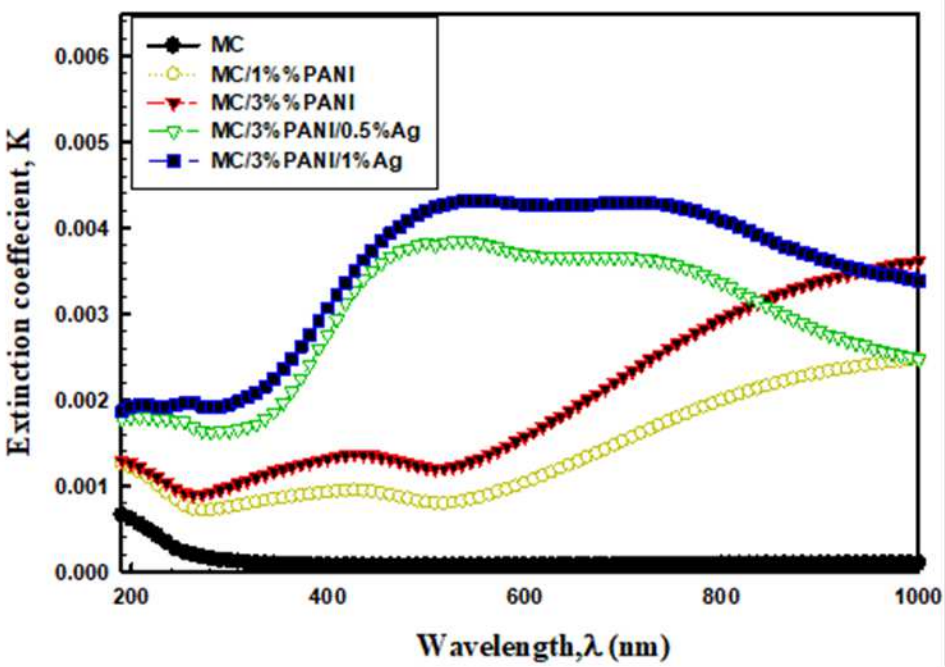

Fig. 7: The extinction coefficient k versus wavelength λ for pristine MC, MC/1%PANI. MC/3%PANI, MC/3%PANI/0.5%Ag and MC/3%PANI/1%Ag films.

Fig.8 shows the relation of the reflectance (R) versus the wavelength (λ) for pristine MC, MC/PANI and MC/PANI/AgNPs films. As noticed, the reflectance R value has enhanced by the addition of PANI and AgNPs. This increase of reflectance R is attributed to reduction of incident light scattering, which reflects the changes of the disorder degree of the polymer chain [35]. This propagation of light through MC/PANI/AgNPs composite based materials has depended on the functional groups of PANI as well as the nature of AgNPs. Furthermore, the behavior change of the reflectance R with PANI and AgNPs, is attributed to the increasing of the packing density of PANI and the AgNPs content in the composite. In other words, the changes of R value have reflected the effects of both PANI and AgNPs for modifying the electronic structure of the MC polymer chain [36].

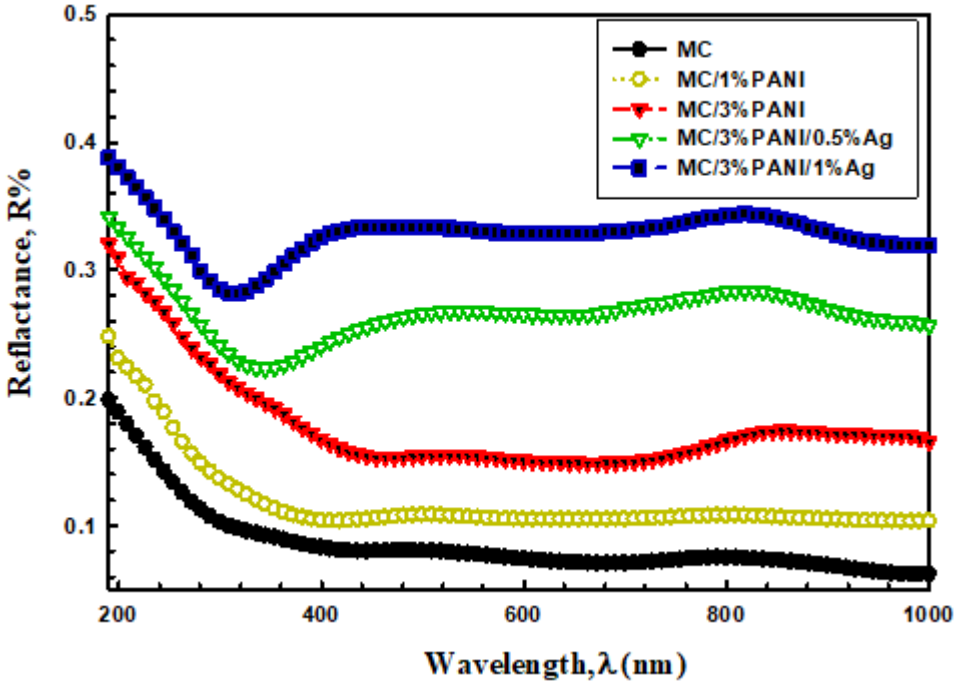

Fig. 8: The reflectance (R) as a function of wavelength (λ) for pristine MC, MC/1%PANI, MC/3%PANI, MC/3%PANI/0.5%Ag and MC/3%PANI/1%Ag films.

The refractive index (*n*), which indicates the electronic polarizability of the ions and the home field into the material is considered as essential one of material characterization properties. Accordingly and in order to deduce the effects of the AgNPs interaction with MC polymer matrix, optical dielectric properties and refractive index are investigated. Fig. 9shows the changes of *n* as a function of wavelength λ for pristine MC, MC/1%PANI, MC/3%PANI, MC/3%PANI/0.5%AgNPs and MC/3%PANI/1%AgNPs films. The refractive index *n* is thus calculated from equation (7) [37]:

$$n = \frac{(1+R)}{(1-R)} + \sqrt{\frac{4R}{(1-R)^2} - K^2} \qquad (7)$$

As can been seen, the *n* is first decreased by wavelength increase for all the films as shown in Fig.9. Next, a steady is observed at the higher wavelengths, demonstrating the normal light dispersion. Furthermore, the refractive index *n* has enhanced by the addition of PANI and AgNPs the the MC polymer chains. This is because localized hesitance of charged particles in the conducting materials. Moreover, the addition of AgNPs and PANI to the MC polymer has improved the film density to make it compact and hard [38]. In other words, the increase the refractive index was a result of the addition of both PANI and AgNPs and their

interaction with the chains of MC which has led to an enhancement in the density of the composite films.

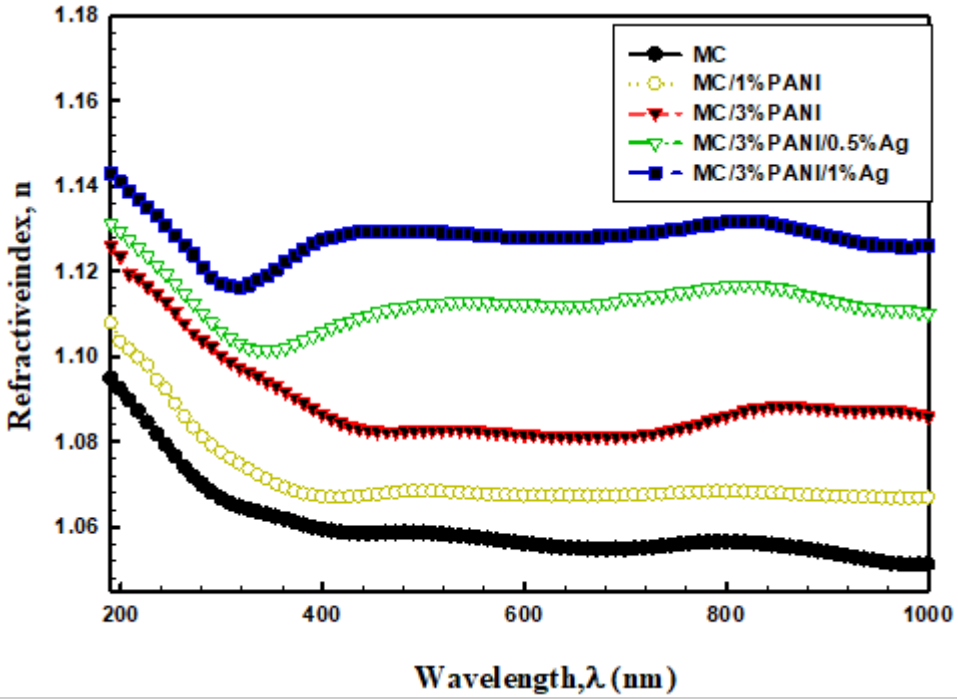

Fig.9. The refractive index n versus wavelength λ of pristine MC, MC/1%PANI, MC/3%PANI, MC/3%PANI/0.5%Ag and MC/3%PANI/1%Ag films.

In order to highlight the optical properties of the newly fabricated MC/PANI/AgNPs composite films, the characteristic dielectric properties have been measured. The dielectric properties are envisioned to give an idea about the polarization behavior of the MC/PANI/AgNPs composite films in the optical devices. In particular we measure the imaginary ε_i and real ε_r dielectric parts which are the most basic material properties that demonstrate the light dispersion of the films. ε_i and ε_r have been determined from equation (8) [39]:

$$\varepsilon = \varepsilon_r + i\varepsilon_i \quad (8)$$

The importance of dielectric constants comes from their roles in presenting valuable information about the energy density states of the prepared materials. The real part ε_r has been estimated from of the refractive index n and extinction coefficient k data using the formula [39]:

$$\varepsilon_r = n^2 - \mathrm{K}^2 \quad (9)$$

The variation of real dielectric constant ε_r versus the wavelength λ for pristine MC, MC/1%PANI, MC/3%PANI, MC/3%PANI/0.5%AgNPs and MC/3%PANI/1%AgNPs films are shown in Fig.10. As can be seen, the real dielectric constant ε_r part has enhanced with increasing both the AgNPs and PANI contents, indicating a good dispersion of PANI and AgNPs into MC polymer chain, because the induced structure changes of Ag and PANI in polymer matrix. By increasing the silver content from 0.5% to 1% into the MC/3%PANI blend, the motion of charge carriers and localized charged particles fluctuations has induced modifications in the optical dielectric dispersion properties, indicating flexible films for optical energy applications.

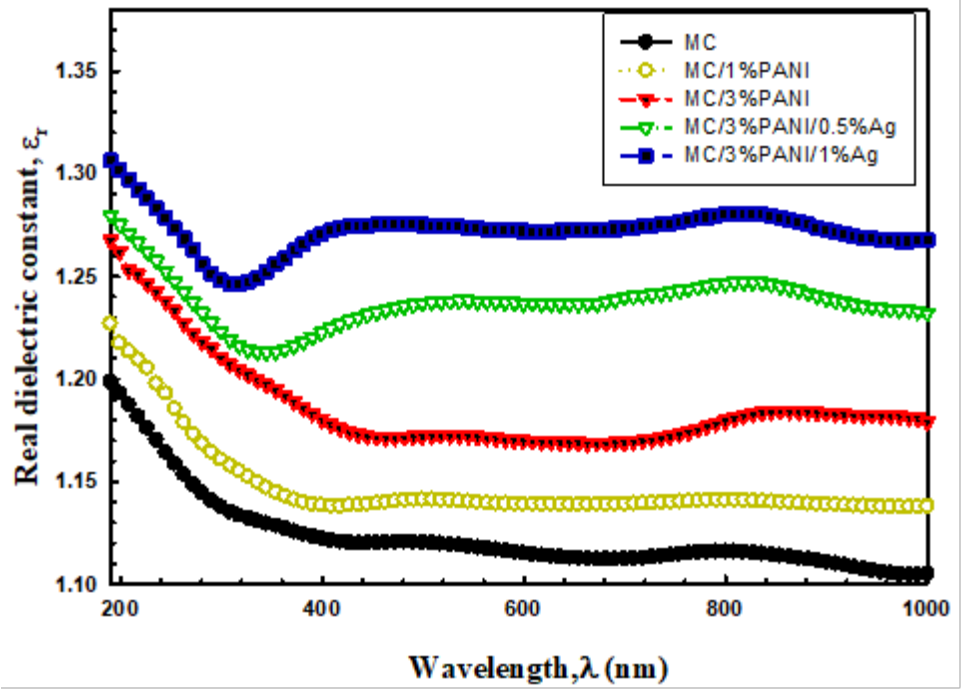

Fig.10: Variation of real dielectric constant ε_r, as a function of wavelength λ of pristine MC, MC/1%PANI, MC/3%PANI, MC/3%PANI/0.5%Ag and MC/3%PANI/1%Ag films.

The imaginary part ε_i , which demonstrate the absorbed energy of electric field as results of dipole moment motion, is given by following equation (equation 10) [39]:

$$\varepsilon_i = 2\,n\,k \qquad (10)$$

The variation of the imaginary dielectric constant (ε_i) as a function of photon energy (hν) of pristine MC, MC/1%PANI, MC/3%PANI, MC/3%PANI/0.5%AgNPs andMC/3%PANI/1%AgNPs films is shown in Fig.11. As noticed, the behavior of ε_i is similar to the behavior of extinction coefficient k. Probably, this is because the refractive index is very tiny. Furthermore, the imaginary part of the dielectric constant mainly depends on the

(k) values which are related to the variation of the absorption coefficients. The imaginary dielectric constant has enhanced bythe addition of PANI and AgNPs into the MC polymer and the MC/PANI blend. This is because the formed defects has induced charge transfer reactions between the MC polymer chains and the AgNPs dopant [40].

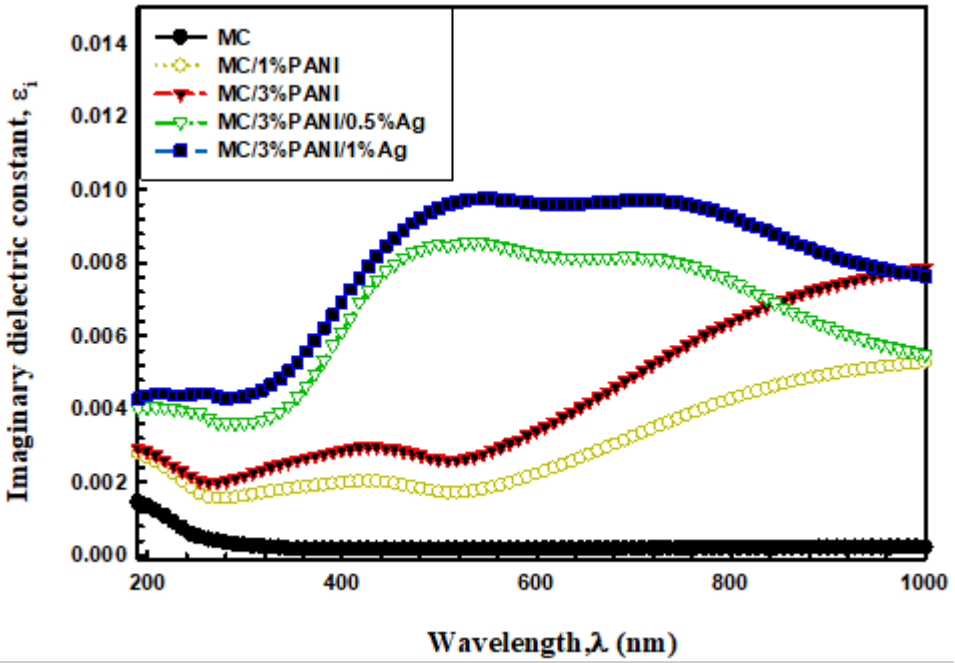

Fig.11: Imaginary dielectric constant (ε_i), as a function of photon energy (hν) for pristine MC, MC/1%PANI, MC/3%PANI, MC/3%PANI/0.5%Ag and MC/3%PANI/1%Ag films.

The refractive index values can be modeled according to the single oscillator paradigm, which suggested by Wemple and DiDomenico as indiacted in equation (11) [41]:

$$\frac{1}{n^2-1} = \frac{E_O}{E_d} - \frac{1}{E_O E_d}(h\nu)^2 \qquad (11)$$

Where, E_o represents the single oscillator energy, and E_d refers to the dispersion energy, which measures the intensity of inter-band transitions and the variations correlating with the structural arrangement of the material. Therefore, by plotting the relation between $(n^2\text{-}1)^{-1}$ and $(h\nu)^2$ of the pristine MC, MC/PANI, and MC/PANI/Ag films as shown in Fig. 12, we can deduce the values of the parameters E_o and E_d through the intercept of y- axe and the slope of the linear fit part, respectively. Additionally, the static refractive index values (n_o) of the pristine MC, MC/PANI, and MC/PANI/Ag films can be computed via extrapolating upright portion of each curve with ordinate $(h\nu)^2 = 0$ as [42]:

$$n_o = (1 + \frac{E_d}{E_O})^{1/2} \qquad (12)$$

The zero frequency of dielectric constants (ε_∞) of the films has been determined by employing the relation $\varepsilon_\infty = (n_o)^2$. The parameters E_o, E_d, and ε_∞ for the pristine MC, MC/PANI, and MC/PANI/Ag films, have been estimated and recorded in Table 2. As noticed the enhancement of dispersion energy from 0.43 for pure MC to 0.87 for MC/3%PANI and to 0.90 for MC/3%PANI/1%Ag implied that the electronic structure of MC molecules has suffered from both the modifications of PANI and AgNPs added to MC, and the defects developed in MC matrix.

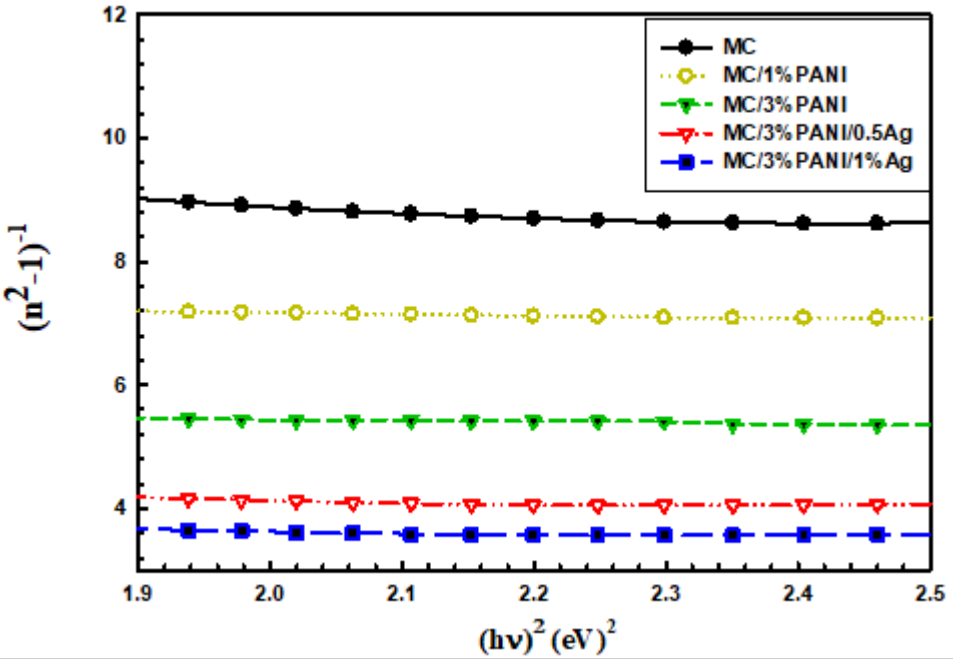

Fig.12: The relation between $(n^2-1)^{-1}$ and $(h\upsilon)^2$ for pristine MC, MC/1%PANI, MC/3%PANI, MC/3%PANI/0.5%Ag and MC/3%PANI/1%Ag films.

Besides, other parameters such as the lattice dielectric constant (ε_l) and the ratio concentration of free carrier and its effective mass (N/m*) can be deduced using another relation of the real part of dielectric constant in Spitzer–Fan model (equation 13) [43]:

$$\varepsilon_r = \varepsilon_l - \left(\frac{e^2}{4\,\pi^2 \varepsilon_s c^2}\frac{N}{m^*}\right)\lambda^2 \qquad (13)$$

Where, c represents the light speed, e defines the charge of an electron and ε_s demonstrates the free space dielectric. Therefore, by plotting the relevance among the real part dielectric

constant and λ^2 for the pristine MC, MC/PANI, and MC/PANI/Ag films as shown in Fig.13. The values of ε_l and N/m* are determined from the intercept of x-axe and the slope of the straight portions, respectively. Furthermore, the plasma resonance frequency values (W_p) for each valence electron involved in the optical transitions is estimated by employing the following equation (equation 14) [44]:

$$W_p = \frac{e^2}{\varepsilon_o} x \frac{N}{m^*} \qquad (14)$$

As noticed from the data of Table 2, the values of ε_l , N/m* and W_p have increased with increasing the contents of both PANI and AgNPs. These increases have been attributed to the variation in bond length with the addition of PANI and AgNPs. In particular, ε_∞ and (N/m^*) values have been reduced with increasing the AgNPs content due to the reduction in the number of dipoles which contributes to the polarization.

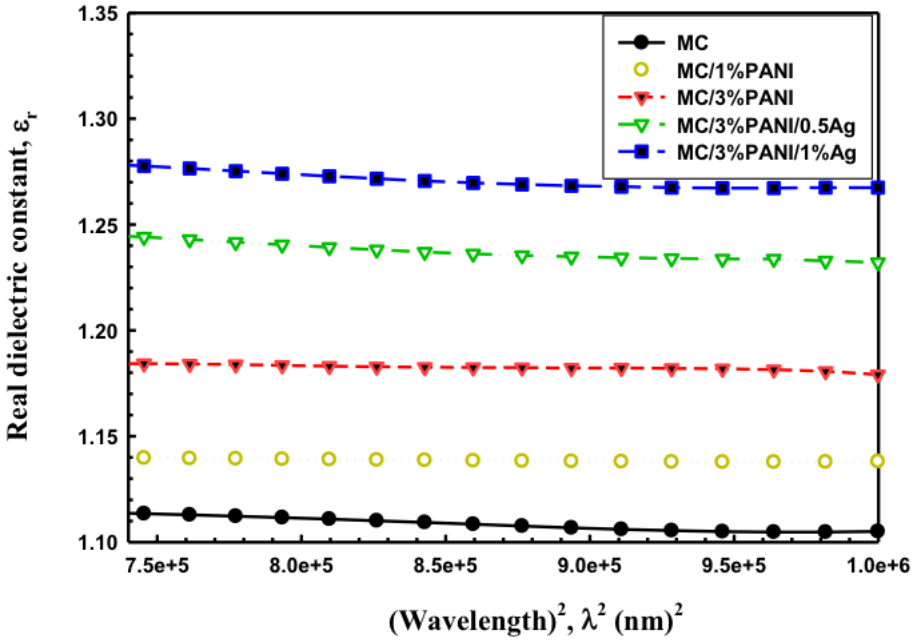

Fig.13: Variation of real dielectric constant (ε_r), as a function of wavelength (λ^2) for pristine MC, MC/1%PANI, MC/3%PANI, MC/3%PANI/0.5%Ag and MC/3%PANI/1%Ag films.

Table. 2. Values of the optical parameters E_o, E_d, ε_∞, ε_l, N/m* and W_p of the pristine MC, MC/1%PANI, MC/3%PANI, MC/3%PANI/0.5Ag and MC/3%PANI/1Ag films.

The samples	E_o (eV)	E_d (eV)	ε_∞	ε_l	$N/m^* x10^{38}$ Kg^{-1} m^{-3}	W_p $x10^{12}$ (Sec^{-1})
Pure MC	4.1	0.43	1.10	1.11	0.40	0.116
MC/1%PANI	5.12	0.74	1.12	1.14	0.25	0.072
MC/3%PANI	4.80	0.87	1.18	1.18	0.20	0.058
MC/3%PANI/0.5%Ag	3.87	0.90	1.23	1.25	0.60	0.171
MC/3%PANI/1%Ag	4.40	0.90	1.19	1.28	0.50	0.150

The long wavelength refractive index (n_∞) and medium oscillator wave longitude (λ_o) of the pristine MC, MC/1%PANI, MC/3%PANI, MC/3%PANI/0.5%AgNPs and MC/3%PANI/1%AgNPs films are determined by analyzing the data of the refractive index utilizing the Sellmeier oscillator equation (equation 15) [45]:

$$(n_\infty^2 - 1)/(n^2 - 1) = 1 - (\frac{\lambda_o}{\lambda})^2 \qquad (15)$$

By studying the relation between $(n^2\text{-}1)^{-1}$ and λ^{-2} at longer wavelength as shown in Fig. 14, the values of n_∞ and λ_o can be obtained from the intercept of the x-axe and the slope of the linear part of the detour, respectively. It is clear from the data of Table 3, that the value of n_∞ and λ increases with increasing contents of both PANI and AgNPs. The λ_o has increased from 477 nm to 500 nm, while the n_o has increased from 1.11 to 1.26 by increasing silver content from 0.5% to 1%. On the other hand, by hiring the single Sellmeier oscillator at depressed energy $(n_o^2\text{-}1/n^2)^{-1} = 1\text{-}(\lambda_o/\lambda)^2$, it was possible to compute the value of oscillator length intensity (S_o) through the following equation (equation 16) [46]:

$$S_o = (n_\infty^2 - 1)/(\lambda_o)^2 \qquad (16)$$

In the Drude model, the imaginary part of dielectric constant ε_i relies on the energy of incident photon and associated with the incident photon wavelength using equation (17)[47]:

$$\varepsilon_i = \frac{1}{4\pi^3\varepsilon_o}\left(\frac{e^2N}{c^3m^*\tau}\right)\lambda^3 \qquad (17)$$

Therefore, the relaxation time values (τ) of all the fabricated films can be determined through the plotting of the ε_i and λ^3 as shown in Fig.15, and listed in Table 3. As can be seen, the time relaxation values gradually decreased with increasing both the PANI and AgNPs. It reduced from 8.8 $x10^{14}$ sec for pure MC to 5.7$x10^{14}$ sec for MC/3%PANI and to 1.1$x10^{14}$ sec

for MC/3%PANI/1%AgNPs. These results confirmed that the formed films have become more convenient to high rapid optoelectronic devices.

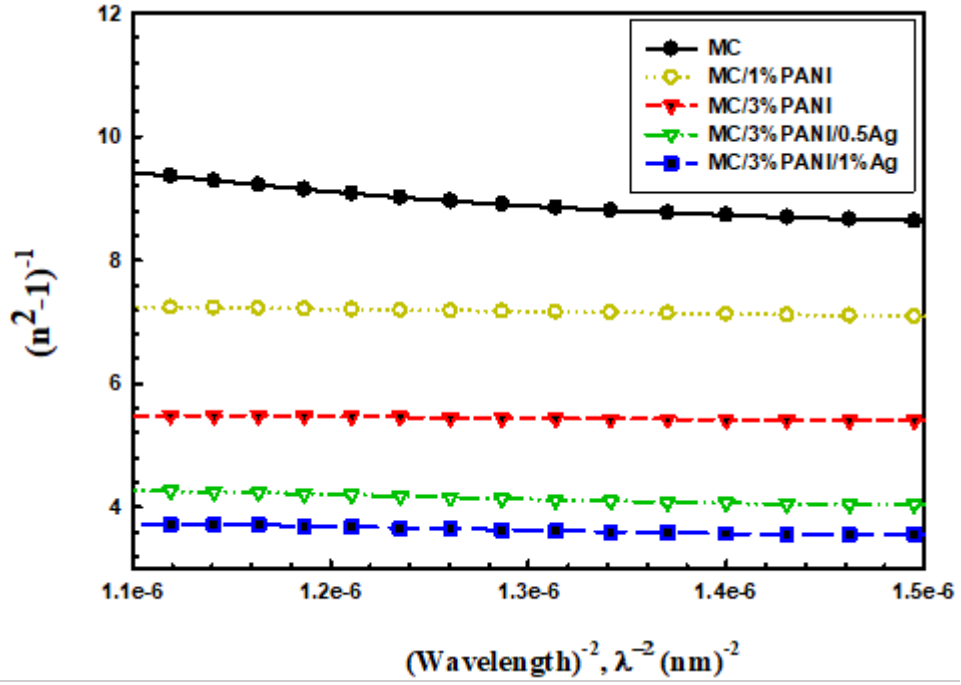

Fig.14: The relation between $(n^2-1)^{-1}$ and $(\lambda)^{-2}$ for pristine MC, MC/1%PANI, MC/3%PANI, MC/3%PANI/0.5%Ag and MC/3%PANI/1%Ag films.

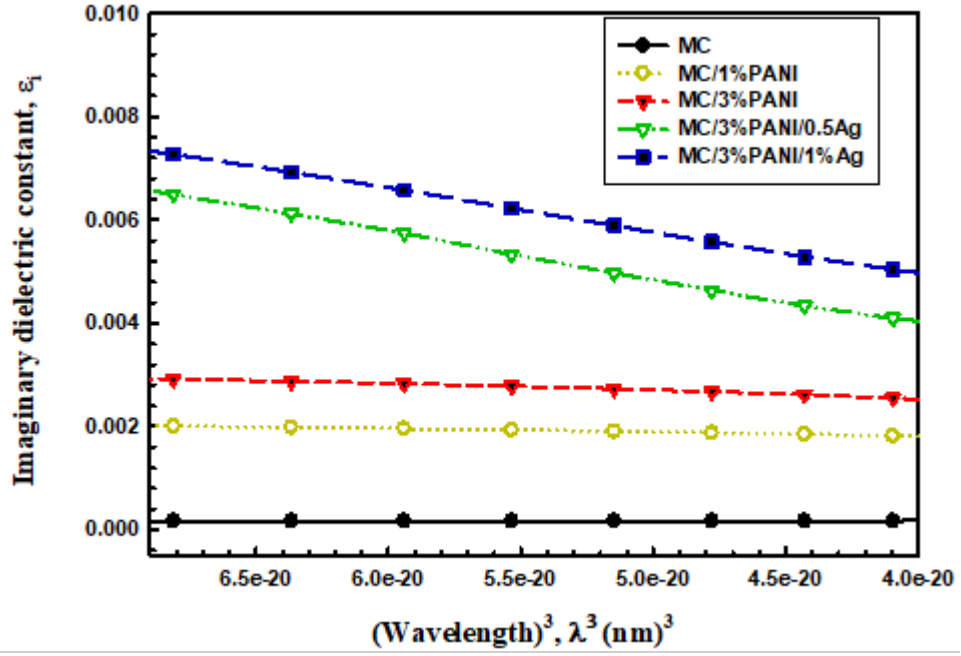

Fig.15. Relation between imaginary dielectric constant ε_i and λ^3 for pristine MC, MC/1%PANI, MC/3%PANI, MC/3%PANI/0.5%Ag and MC/3%PANI/1%Ag films.

The optical conductivity (σ_{opt}) which demonstrates the electrical conductivity that produced as a result of the charge carrier's transfer due to the variation in the electric field of the fallen electromagnetic waves has been determined from absorption coefficient (α) using equation (18) [48]:

$$\sigma_{opt} = \frac{\alpha n c}{4\pi} \qquad (18)$$

Where n refers to the refractive index and c represents the speed of light. The variation of optical conductivity with photon energy is shown in Fig.16. At high photon energy, we can witness the increase of the optical conductivity of films because the high absorbance value in that region has led to increases of the charge transfer excitations. On the other hand, the optical conductivity has increased with increasing both the PANI and AgNPs, due to the increases of the localized stage densities in the band structure. That has led to an increase in the absorption coefficient. This result supports a good miscibility between AgNPs and MC chains as showed by XRD analysis. Furthermore, the enhancement of the optical conductivity (σ_{opt}) and the decrease of the band gap E_g with increasing both the AgNPs and PANI content inside MC has revealed that both the dielectric and the optical measurements are in approval with each other. The optical dielectric properties and the optical conductivity data have reflected the importance the MC/PANI/Ag composite films for optical energy devices.

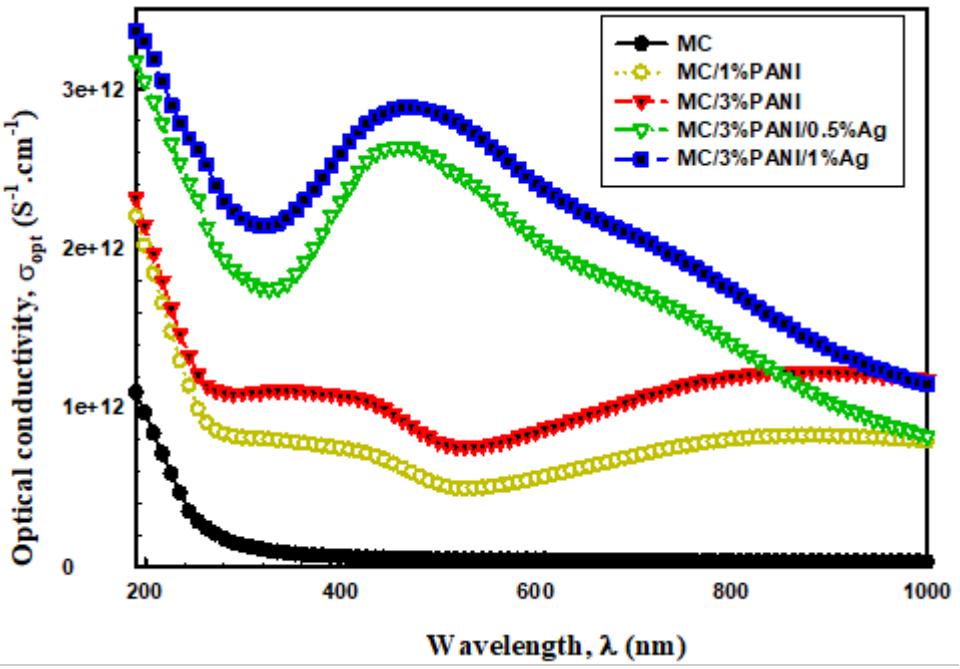

Fig.16: Variation of optical conductivity with photon energy for pristine MC, MC/1%PANI, MC/3%PANI, MC/3%PANI/0.5AgNPs and MC/3%PANI/1AgNPs films.

Table. 3. Values of the optical parameters W_p, n_∞, λ_o, S_o, and τ of the pristine MC, MC/1%PANI, MC/3%PANI, MC/3%PANI/0.5Ag and MC/3%PANI/1Ag films.

The films	n_o	λ_o (nm)	$S_o x10^{12}$ (m^{-2})	τ x 10^{-14} (sec)
Pure MC	1.05	412	0.58	8.8
MC/1%PANI	1.07	244	2.38	6.6
MC/3%PANI	1.18	346	3.20	5.7
MC/3%PANI/0.5%Ag	1.11	477	1.02	1.4
MC/3%PANI/1%Ag	1.26	500	2.35	1.1

When light waves passes inside the polymer material, it interacts with charge particle of that material and produces a dipole movement. This dipole movement gives the non-linear electron polarizability (P). Accordingly, the composite films has possessed an optical nonlinearity (NLO) and rapid response time. In this study, the NLO of the fabricated films can be featured by equation (19) [49]:

$$P = X^{(1)}E + X^{(2)}E^2 + X^{(3)}E^3 \qquad (19)$$

where P defines polarization of the material, $X^{(1)}$ represents the linear susceptibility, $X^{(2)}$ related to the second order NLO susceptibility which corresponding to a second harmonic generation, and) $X(3)$ refer to the third order NLO susceptibility. Thus, it was possible to calculate the values of $X^{(1)}$ and $X^{(3)}$ by using the following relations (equations 20 and 21) [50]:

$$X^{(1)} = \frac{(n^2-1)}{4\pi} \qquad (20)$$

$$X^{(3)} = A(X^{(1)})^4 \quad (21)$$

The refractive index can thus be written in the following form [50].

$$n(\lambda) = n_o(\lambda) + n_2(E^2) \quad (22)$$

n_o refer to a linear refractive index, n_2 represents NLO refractive index. The values of NLO refractive index from the NLO susceptibility and refractive index (n) can be extracted from the following relation [50]:

$$n_2 = \frac{12\pi X^{(3)}}{n_o} \qquad (23)$$

Where, $n_o = n$, because $n_o >> n_2$. The change of $X^{(1)}$ and $X^{(3)}$ versus wavelength (λ) are depicted in Figs.17a and 17b, respectively of pristine MC, MC/1%PANI, MC/3%PANI, MC/3%PANI/0.5AgNPs and MC/3%PANI/1%AgNPs films. Notably, the values of $X^{(1)}$ and$X^{(3)}$ have increased with increasing both the PANI and AgNPs contents.

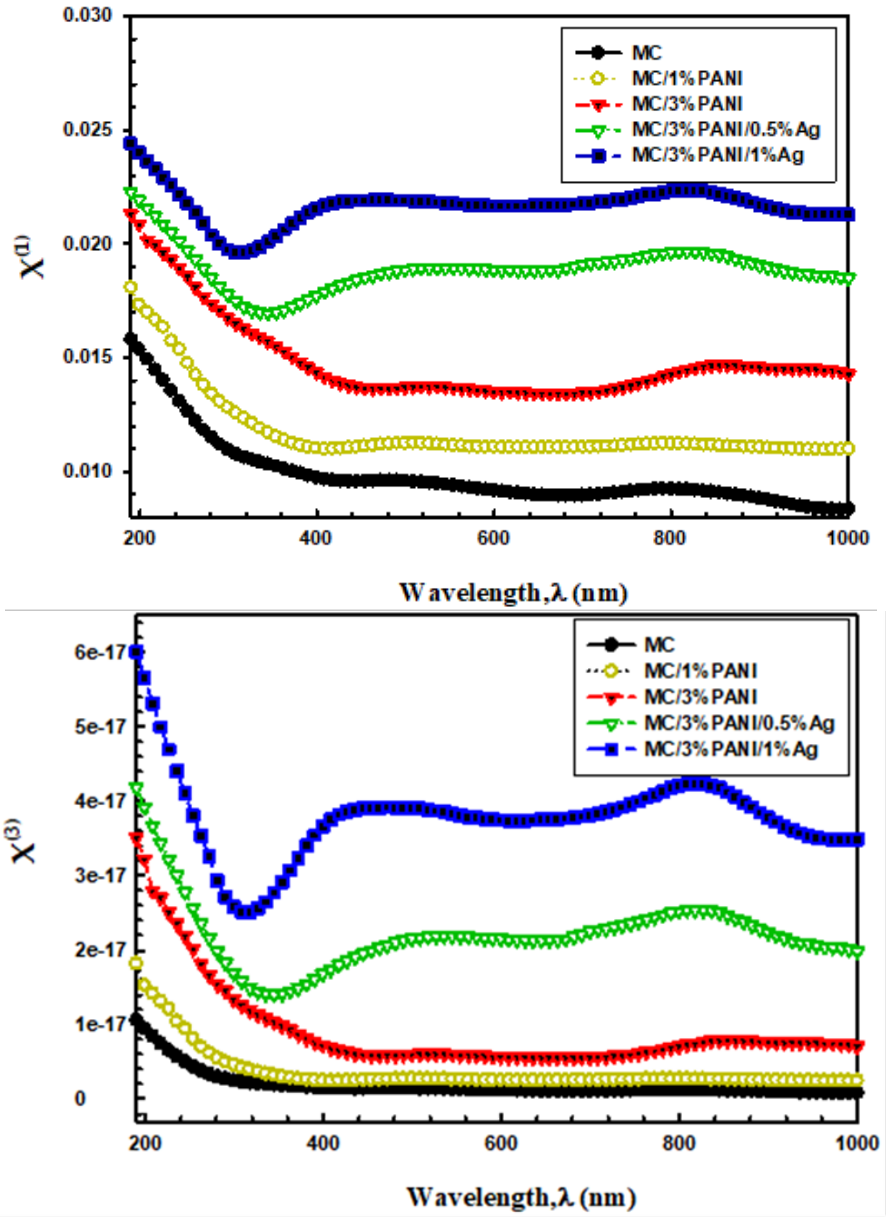

Fig. 17. (a). Linear optical susceptibility$X^{(1)}$ and (b) Non-linear optical susceptibility $X^{(3)}$ as a function of wavelength (λ) of pristine MC, MC/1%PANI, MC/3%PANI, MC/3%PANI/0.5%Ag and MC/3%PANI/1%Ag films.

This increase was due to the creation of defect centers, which has led to a boost local polarizability. Moreover, the increase of $X^{(1)}$ and $X^{(3)}$ with increasing PANI and Ag contents has been attributed to the increase in the interaction of AgNPs with PANI/MC blend that resulted in an enhanced π-π* and n- π* transitions [51]. This result showed the advantages of fabrication composite films composed of PANI and AgNPs, which envisioned to enhance the absorption for the optical devices.

In addition, Fig. 18 has depicted the change of non-linear refractive index against wavelength of the pristine MC, MC/1%PANI, MC/3%PANI, MC/3%PANI/0.5AgNPs and MC/3%PANI/1AgNPs films. Notably, the values of n_2 have the same trend of the valued of $\chi^{(3)}$, as it gradually increased with increasing both the PANI and AgNPs content. These results clearly showed the importance of adding the conducting PANI and AgNPs to MC where the resultant films have indicted an improvement in the nonlinear optical parameters which is favoured for the of the optoelectronic device applications [52].

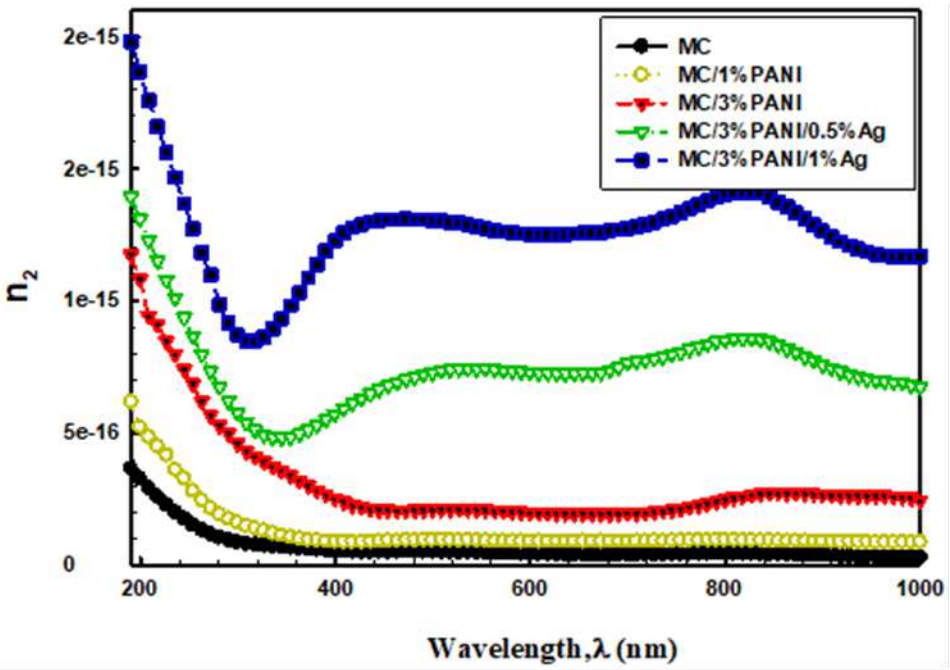

Fig: 18. Non-linear refractive index (n_2) as a function of wavelength (λ) of pristine MC, MC/1%PANI, MC/3%PANI, MC/3%PANI/0.5%Ag and MC/3%PANI/1%Ag films.

4. Conclusion:

MC/PANI blends and MC/PANI/AgNPs composite films were successfully synthesized using the casting reduction method. The linear/nonlinear optical parameters (extinction coefficient, refractive index, reflectance, first order linear optical susceptibility, real and imaginary dielectric constant, and third order nonlinear optical susceptibility) of MC/PANI/AgNPs composite films have been determined using the UV–Vis spectroscopy. The XRD results showed successful fabrications of MC/PANI/AgNPs composite films, with AgNPs crystallite size of 13 nm. The optical energy band gap and the absorption edge of the MC film decreased by the addition of both the PANI and AgNPs. In the meantime, the band tail and the number of carbon clusters of the samples increased with the PANI and AgNPs contents. Moreover, the refractive index and optical dielectric constants changed by increasing both the PANI and AgNPs. On the other hand, the optical conductivity of the prepared films increased by doping the MC polymer by the PANI and AgNPs due to the increased localized stage density in the band structure. The refractive index and the related dispersion parameters of MC, MC/PANI blends and MC/PANI/AgNPs composite films have been calculated and elucidated by using the Wemple-DiDomenico model. By increasing silver content from 0.5% to 1%, the motion of charge carriers and localized charged particles fluctuations produced modifications in the optical dielectric dispersion properties. The results indicate that the prepared films can be considered as promising flexible materials for optical energy applications.

Acknowledgement

The authors extend their appreciation to the Deputyship for Research Innovation, Ministry of Education in Saudi Arabia for funding this work through the project number "375213500". The authors also would like to extend their sincere appreciation to the central laboratory at Jouf University for supporting this study.

References

1- Zhang, T., Cheng, Q., Jiang, B., & Huang, Y. (2020). Design of the novel polyaniline/polysiloxane flexible nanocomposite film and its application in gas sensor. Composites Part B: Engineering, 196, 108131.

2- Lotfy, S., Atta, A., & Abdeltwab, E. (2018). Comparative study of gamma and ion beam irradiation of polymeric nanocomposite on electrical conductivity. Journal of Applied Polymer Science, 135(15), 46146.

3- Shandilya, M., Thakur, S., & Thakur, S. (2020). Magnetic amendment in the fabrication of environment friendly and biodegradable iron oxide/ethyl cellulose nanocomposite membrane via electrospinning. Cellulose, 27(17), 10007-10017.

4- Chen, B., Sun, Q., Wang, D., Zeng, X. F., Wang, J. X., & Chen, J. F. (2020). High-gravity-assisted synthesis of surfactant-free transparent dispersions of monodispersed MgAl-LDH nanoparticles. Industrial & Engineering Chemistry Research, 59(7), 2960-2967.

5- Das, M., & Sarker, A. K. (2020). Multilayer Engineering of Polyaniline and Reduced Graphene Oxide Thin Films on a Plastic Substrate for Flexible Optoelectronic Applications Using NIR. Russian Journal of Applied Chemistry, 93(10), 1561-1570.

6- Nadour, M., Boukraa, F., Ouradi, A., & Benaboura, A. (2017). Effects of methylcellulose on the properties and morphology of polysulfone membranes prepared by phase inversion. Materials Research, 20(2), 339-348.

7- Liebeck, B. M., Hidalgo, N., Roth, G., Popescu, C., & Böker, A. (2017). Synthesis and characterization of methyl cellulose/keratin hydrolysate composite membranes. Polymers, 9(3), 91.

8- Sun, Jing, et al. "A novel flexible Ag/AgCl quasi-reference electrode based on silver nanowires toward ultracomfortable electrophysiology and sensitive electrochemical glucose detection." Journal of Materials Research and Technology 9.6 (2020): 13425-13433.

9- Lu, Z., Yao, C., Xie, F., Si, L., Jia, F., Huang, J., ... & Ma, Q. (2020). Highly flexible and conductive sodium carboxymethyl cellulose/silver nanowires composite films. Journal ofMaterials Science: Materials in Electronics, 31(3), 2353-2359.

10- Ren, Z., Chen, F., Wen, K., & Lu, J. (2020). Enhanced photocatalytic activity for tetracyclines degradation with Ag modified g-C3N4 composite under visible light. Journal of Photochemistry and Photobiology A: Chemistry, 389, 112217.

11- Zhang, J., Li, H., Xu, T., Wu, J., Zhou, S., Hang, Z. H., ... & Yang, Z. (2020). Homogeneous silver nanoparticles decorating 3D carbon nanotube sponges as flexible high-performance electromagnetic shielding composite materials. Carbon, 165, 404-411.

12- M. Abdelhamied, A. Atta, A. Abdelreheem, A. Farag, and M. El Okr, "Synthesis and Optical Properties of PVA/PANI/Ag Nanocomposite films," Journal of Materials Science: Materials in Electronics, pp. 1-13, 2020.

13- Lu, Y., Song, Y., & Wang, F. (2013). Thermoelectric properties of graphene nanosheets-modified polyaniline hybrid nanocomposites by an in situ chemical polymerization. Materials Chemistry and Physics, 138(1), 238-244.

14- Abdel-Wahab, M. S., Jilani, A., Yahia, I. S., & Al-Ghamdi, A. A. (2016). Enhanced the photocatalytic activity of Ni-doped ZnO thin films: Morphological, optical and XPS analysis. Superlattices and microstructures, 94, 108-118.

15-Hebeish, A., & Sharaf, S. (2015). Novel nanocomposite hydrogel for wound dressing and other medical applications. *RSC advances*, *5*(125), 103036-103046.

16- Butoi, B., Groza, A., Dinca, P., Balan, A., & Barna, V. (2017). Morphological and structural analysis of polyaniline and poly (o-anisidine) layers generated in a DC glow discharge plasma by using an oblique angle electrode deposition configuration. *Polymers*, *9*(12), 732.

17- Zafar, S., & Zafar, A. (2019). Biosynthesis and characterization of silver nanoparticles using Phoenix dactylifera fruits extract and their in vitro antimicrobial and cytotoxic effects. *The Open Biotechnology Journal*, *13*(1).

18-Cho, S., Lee, J. S., & Joo, H. (2019). Recent developments of the solution-processable and highly conductive polyaniline composites for optical and electrochemical applications. Polymers, 11(12), 1965.

19- Sezer, A., Gurudas, U., Collins, B., Mckinlay, A., & Bubb, D. M. (2009). Nonlinear optical properties of conducting polyaniline and polyaniline–Ag composite thin films. Chemical Physics Letters, 477(1-3), 164-168

20- Jebur Q, Hashim A, Habeeb M. Fabrication, Structural and Optical properties for (Polyvinyl Alcohol–Polyethylene Oxide–Iron Oxide) Nanocomposites. Egyptian Journal of Chemistry. 2020;63(2):611-23.

21- Abdel-Galil A, Atta A and Balboul MR. Effect of low energy oxygen ion beam treatment on the structural and physical properties of ZnO thin films. Surface Review and Letters (2020).

22- K. M. Chintala, S. Panchal, P. Rana, and R. Chauhan, "Structural, optical and electrical propertie of gamma-rays exposed selenium nanowires," Journal of Materials Science: Materials in Electronics, vol. 27, pp. 8087-8093, 2016.

23- A. Abdel-Galil, M. Assiri, and I. Yahia, "Optical analysis of methyl violet thin films/polymeric substrate for flexible organic technology," Optical and Quantum Electronics, vol. 52, pp. 1-20, 2020

24- Atta A, ABDEL REHEEM AM, and Abdeltwab E. Ion Beam Irradiation Effects on Surface Morphology and Optical Properties of ZnO/PVA Composites. Surface Review and Letters (2020): 1950214.

25- Soliman T, Abouhaswa A. Synthesis and structural of Cd0. 5Zn0. 5F2O4 nanoparticles and its influence on the structure and optical properties of polyvinyl alcohol films. Journal of Materials Science: Materials in Electronics. 2020;31(12):9666-74.

26- wad S, El-Gamal S, El Sayed AM, Abdel-Hady EE. Characterization, optical, and nanoscale free volume properties of Na-CMC/PAM/CNT nanocomposites. Polymers for Advanced Technologies. 2020;31(1):114-25.

27- Shen, D., Wu, Y., Lo, M. F., & Lee, C. S. (2020). Charge transport properties of co-evaporated organic–inorganic thin film charge transfer complexes: effects of intermolecular interactions. *Journal of Materials Chemistry C*, *8*(47), 16725-16729.

28- Ledinsky M, Schönfeldová T, Holovský J, Aydin E, Hájková Zk, Landová L, et al. Temperature dependence of the urbach energy in lead iodide perovskites. The journal of physical chemistry letters. 2019;10(6):1368-73.

29- Abdel-Galil, A., Balboul, M. R., Atta, A., Yahia, I. S., & Sharaf, A. (2014). Preparation, structural and optical characterization of nanocrystalline CdS thin film. *Physica B: Condensed Matter*, *447*, 35-41.

30- H. Zeyada, M. El-Nahass, and M. El-Shabaan, "Gamma-ray irradiation induced structural and optical constants changes of thermally evaporated neutral red thin films," Journal of Materials Science, vol. 47, pp. 493-502, 2012.

31- Abdel Reheem AM, Atta A, Afify TA. Optical and electrical properties of argon ion beam irradiated PVA/Ag nanocomposites. Surface Review and Letters.2017; 24(03): 1750038.

32- Yahia, I. S., Alfaify, S., Jilani, A., Abdel-wahab, M. S., Al-Ghamdi, A. A., Abutalib, M. M., ... & El-Naggar, A. M. (2016). Non-linear optics of nano-scale pentacene thin film. Applied Physics B, 122(7), 1-5.

33- Jilani, A., Othman, M. H. D., Ansari, M. O., Hussain, S. Z., Ismail, A. F., & Khan, I. U. (2018). Graphene and its derivatives: synthesis, modifications, and applications in wastewater treatment. Environmental Chemistry letters, 16(4), 1301-1323.

34- Kravets, V. G., Marshall, O. P., Nair, R. R., Thackray, B., Zhukov, A., Leng, J., & Grigorenko, A. N. (2015). Engineering optical properties of a graphene oxide metamaterial assembled in microfluidic channels. Optics express, 23(2), 1265-1275.

35- Taha, T. A., Hendawy, N., El-Rabaie, S., Esmat, A., & El-Mansy, M. K. (2019). Effect of NiO NPs doping on the structure and optical properties of PVC polymer films. *Polymer Bulletin*, *76*(9), 4769-4784.

36- Ghanipour M, Dorranian D. Effect of Ag-nanoparticles doped in polyvinyl alcohol on the structural and optical properties of PVA films. Journal of Nanomaterials. 2013;2013.

37- Barde, R. V., Nemade, K. R., & Waghuley, S. A. (2016). Complex optical study of V2O5–P2O5–B2O3–Dy2O3 glass systems. Journal of Taibah University for Science, 10(3), 340-344.

38- Singh D, Kumar S, Thangaraj R. Optical properties of polyvinyl alcohol doped (Se80Te20) 100–x Ag x (0≤ x≤ 4) composites. Phase Transitions. 2014;87(2):206-22.

39- Donya H, Taha T, Alruwaili A, Tomsah I, Ibrahim M. Micro-structure and optical spectroscopy of PVA/iron oxide polymer nanocomposites. Journal of Materials Research and Technology. 2020;9(4):9189-94.

40- Ghanipour M, Dorranian D. Effect of Ag-nanoparticles doped in polyvinyl alcohol on the structural and optical properties of PVA films. Journal of Nanomaterials. 2013;2013.

41- M. El-Nahass, A. Farag, and F. Abd-El-Salam, "Effect of gamma irradiation on the optical properties of nano-crystalline InP thin films," Applied surface science, vol. 255, pp. 9439-9443, 2009.

42- Ali, F. M., Kershi, R. M., Sayed, M. A., & AbouDeif, Y. M. (2018). Evaluation of structural and optical properties of Ce3+ ions doped (PVA/PVP) composite films for new organic semiconductors. *Physica B: Condensed Matter*, *538*, 160-166.

43-T. J. Alwan, "Gamma irradiation effect on the optical properties and refractive index dispersion of dye doped polystyrene films," Turkish Journal of Physics, vol. 36, pp. 377-384, 2012.

44- A. El Sayed, S. El-Sayed, W. Morsi, S. Mahrous, and A. Hassen, "Synthesis, characterization, optical, and dielectric properties of polyvinyl chloride/cadmium oxide nanocomposite films," Polymer composites, vol. 35, pp. 1842-1851, 2014.

45- I. Saadeddin, B. Pecquenard, J.-P. Manaud, R. Decourt, C. Labrugère, T. Buffeteau, et al., "Synthesis and characterization of single-and co-doped SnO2 thin films for optoelectronic applications," Applied Surface Science, vol. 253, pp. 5240-5249, 2007.

46- M. H. Hassouni, K. A. Mishjil, S. S. Chiad, and N. F. Habubi, "Effect of gamma irradiation on the optical properties of Mg doped CdO Thin films deposited by Spray Pyrolysis," International Letters of Chemistry, Physics and Astronomy, vol. 11, 2013.

47- M. B. Mohamed and M. Abdel-Kader, "Effect of excess oxygen content within different nano-oxide additives on the structural and optical properties of PVA/PEG blend," Applied Physics A, vol. 125, p. 209, 2019.

48- M. Frumar, J. Jedelský, B. Frumarova, T. Wagner, and M. Hrdlička, "Optically and thermally induced changes of structure, linear and non-linear optical properties of chalcogenides thin films," Journal of non-crystalline solids, vol. 326, pp. 399-404, 2003.

49- Jilani, A., Abdel-wahab, M. S., Al-ghamdi, A. A., sadik Dahlan, A., & Yahia, I. S. (2016). Nonlinear optical parameters of nanocrystalline AZO thin film measured at different substrate temperatures. Physica B: Condensed Matter, 481, 97-103.

50- Kaur, R., Singh, K. P., & Tripathi, S. K. (2020). Study of linear and non-linear optical responses of MoSe 2–PMMA nanocomposites. *Journal of Materials Science: Materials in Electronics*, *31*(22), 19974-19988.

51- S. K. Sen, A. Al Mortuza, M. Manir, M. Pervez, S. Hossain, M. S. Alam, et al., "Structural and optical properties of sol-gel synthesized h-MoO3 nanorods treated by gamma radiation," Nano Express, vol. 1, p. 020026, 2020.

52- Ravi, S., Sreedharan, R., Raghi, K. R., Kumar, T. M., & Naseema, K. (2020). Experimental and computational perspectives on linear and non-linear optical parameters of an orthorhombic crystal for optical limiting applications. *Applied Physics A*, *126*(1), 1-19.

53- Heidari, B., Salmani, S., Ghamsari, M. S., Ahmadi, M., & Majles-Ara, M. H. (2020). Ag/PVP nanocomposite thin film with giant optical nonlinearity. *Optical and Quantum Electronics*, *52*(2), 1-18.

Figures

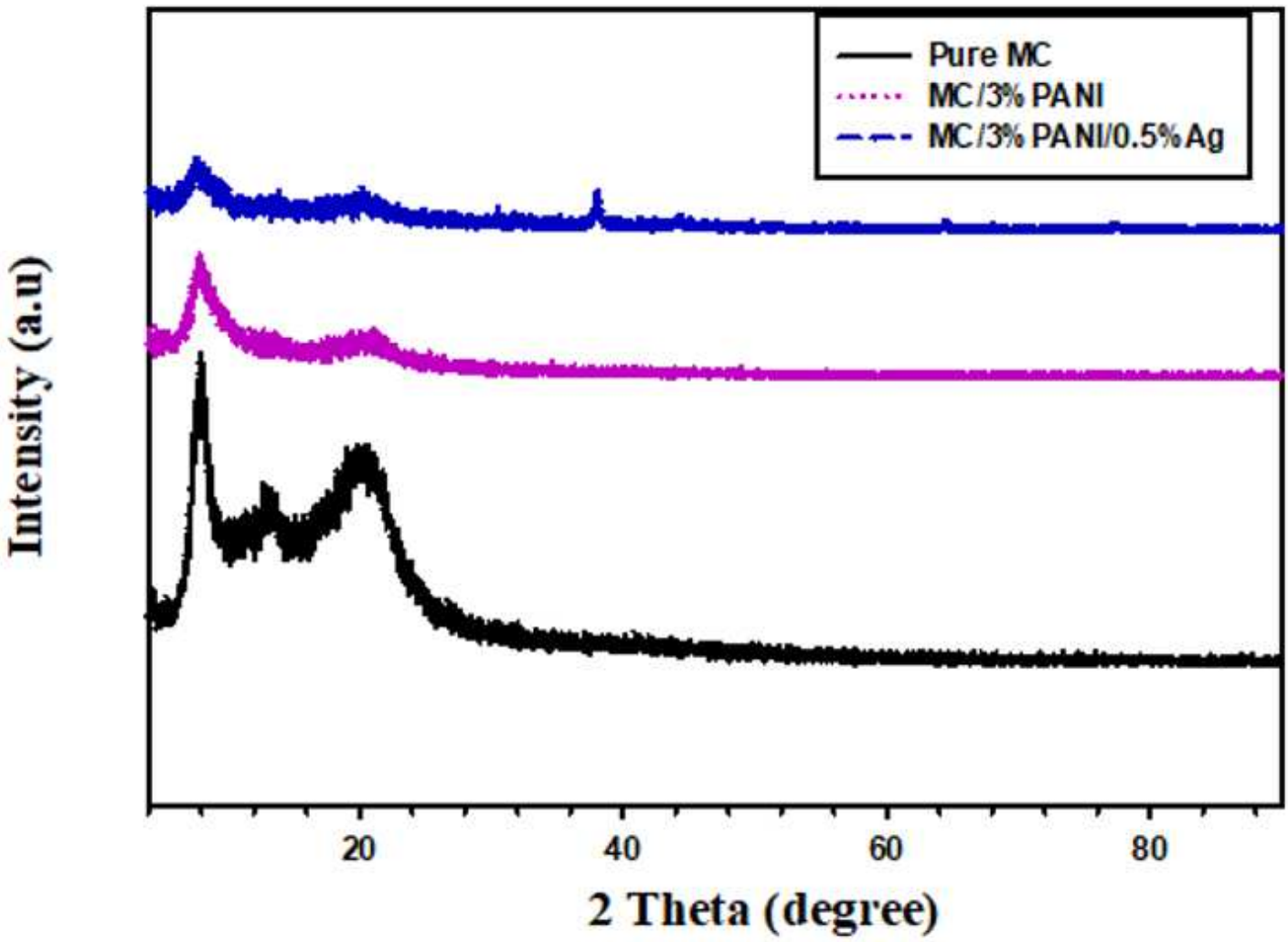

Figure 1

XRD patterns of pristine MC, MC/3%PANI and MC/3%PANI/0.5Ag films

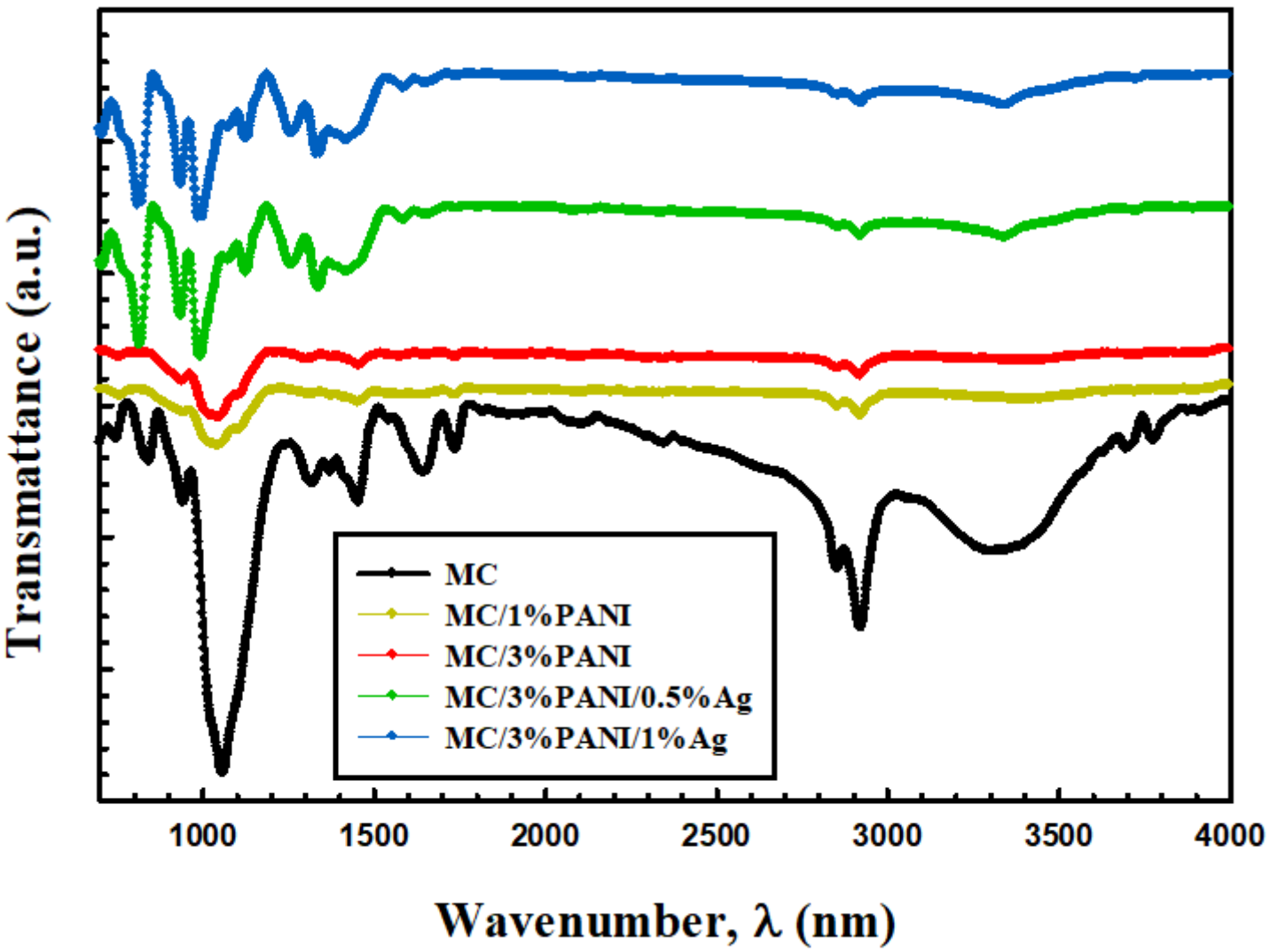

Figure 2

IR spectra of pristine MC, MC/1%PANI, MC/3%PANI, MC/3%PANI/0.5%Ag and MC/3%PANI/0.5Ag films

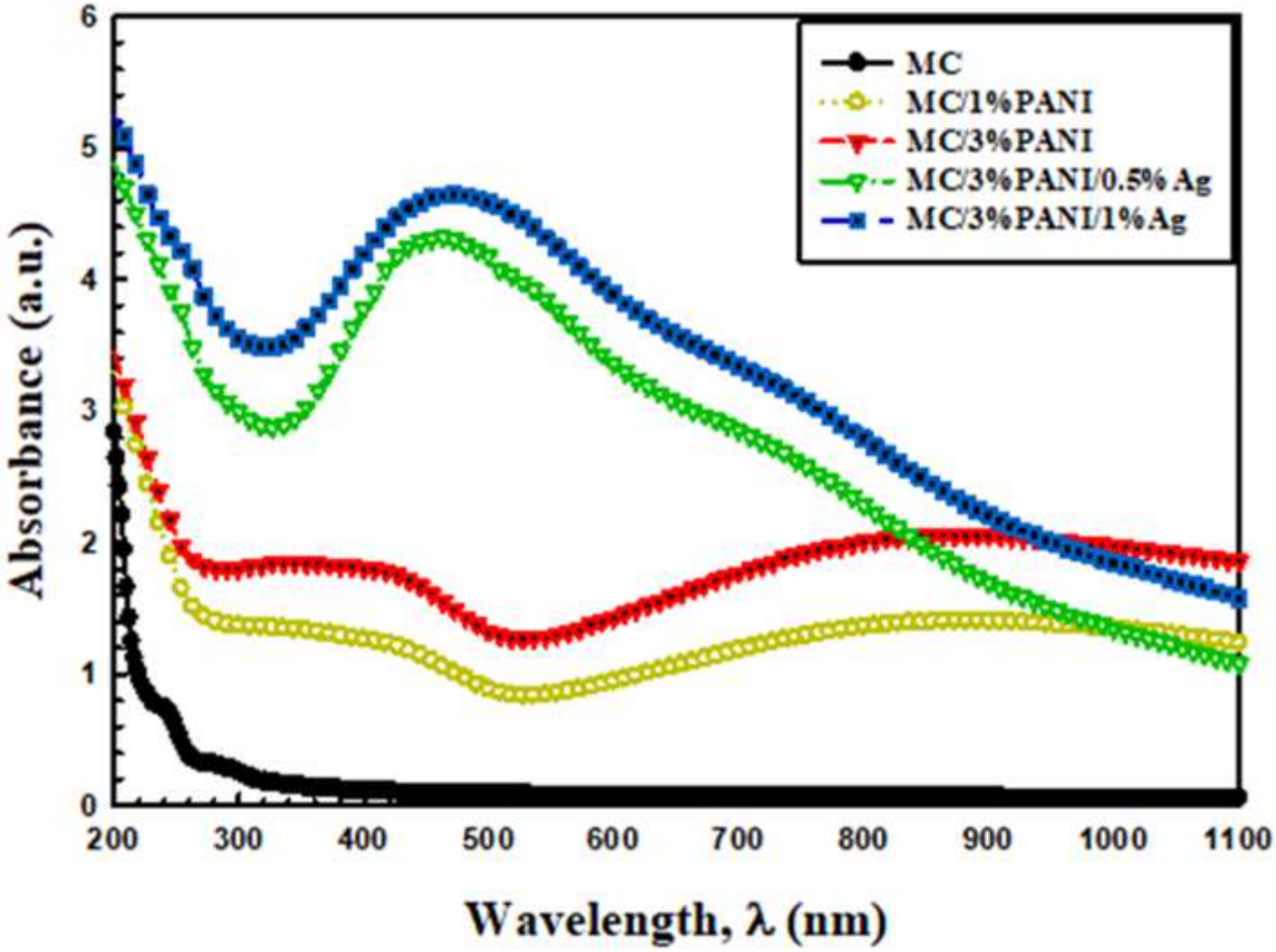

Figure 3

UV-Vis Absorption spectra of pristine MC, MC/1%PANI, MC/3%PANI, MC/3%PANI/0.5%Ag and MC/3%PANI/1%Ag films.

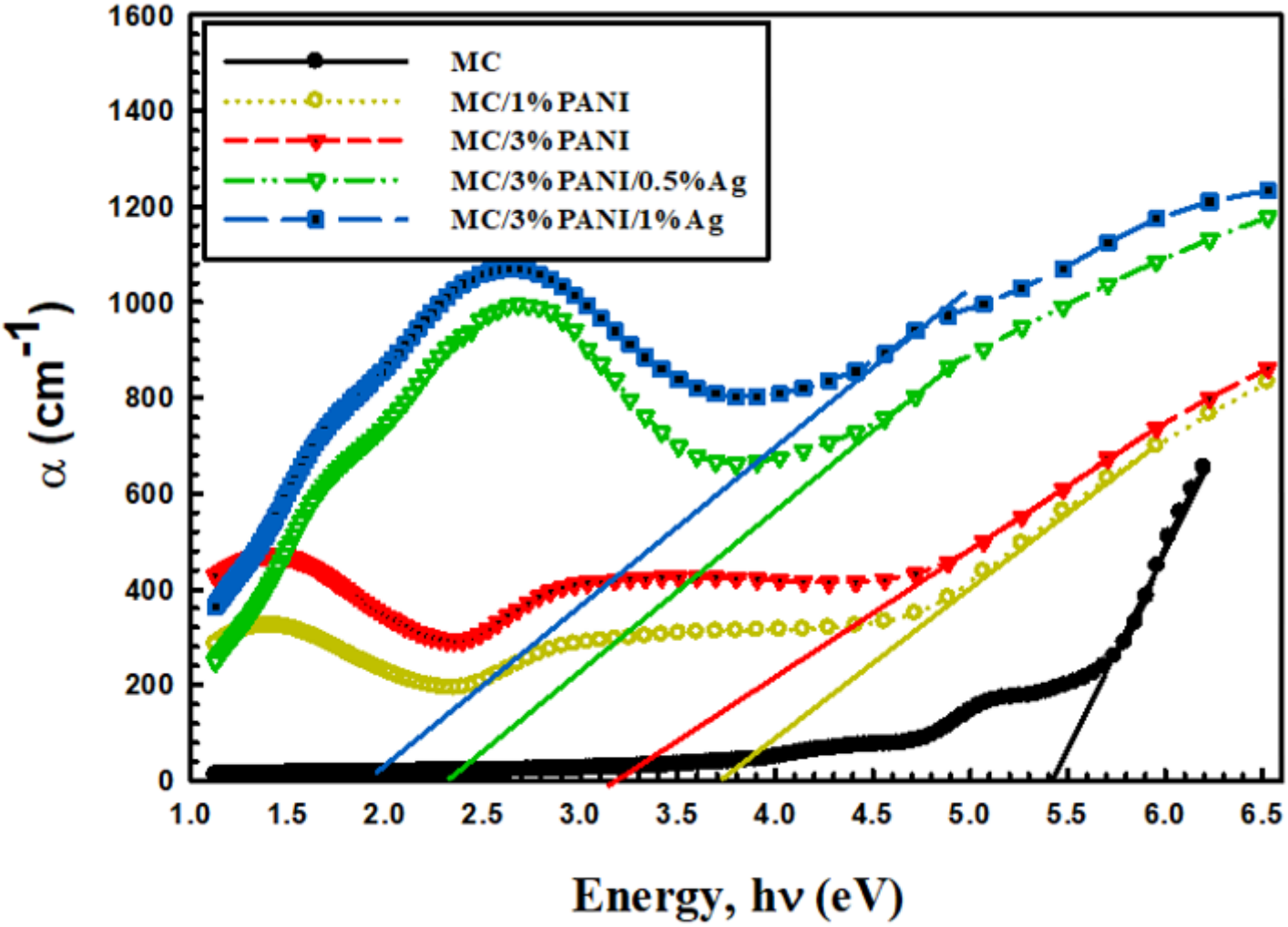

Figure 4

Absorption coefficients α as a function of wavelength for pristine MC, MC/1%PANI, MC/3%PANI, MC/3%PANI/0.5%Ag and MC/3%PANI/1%Ag films

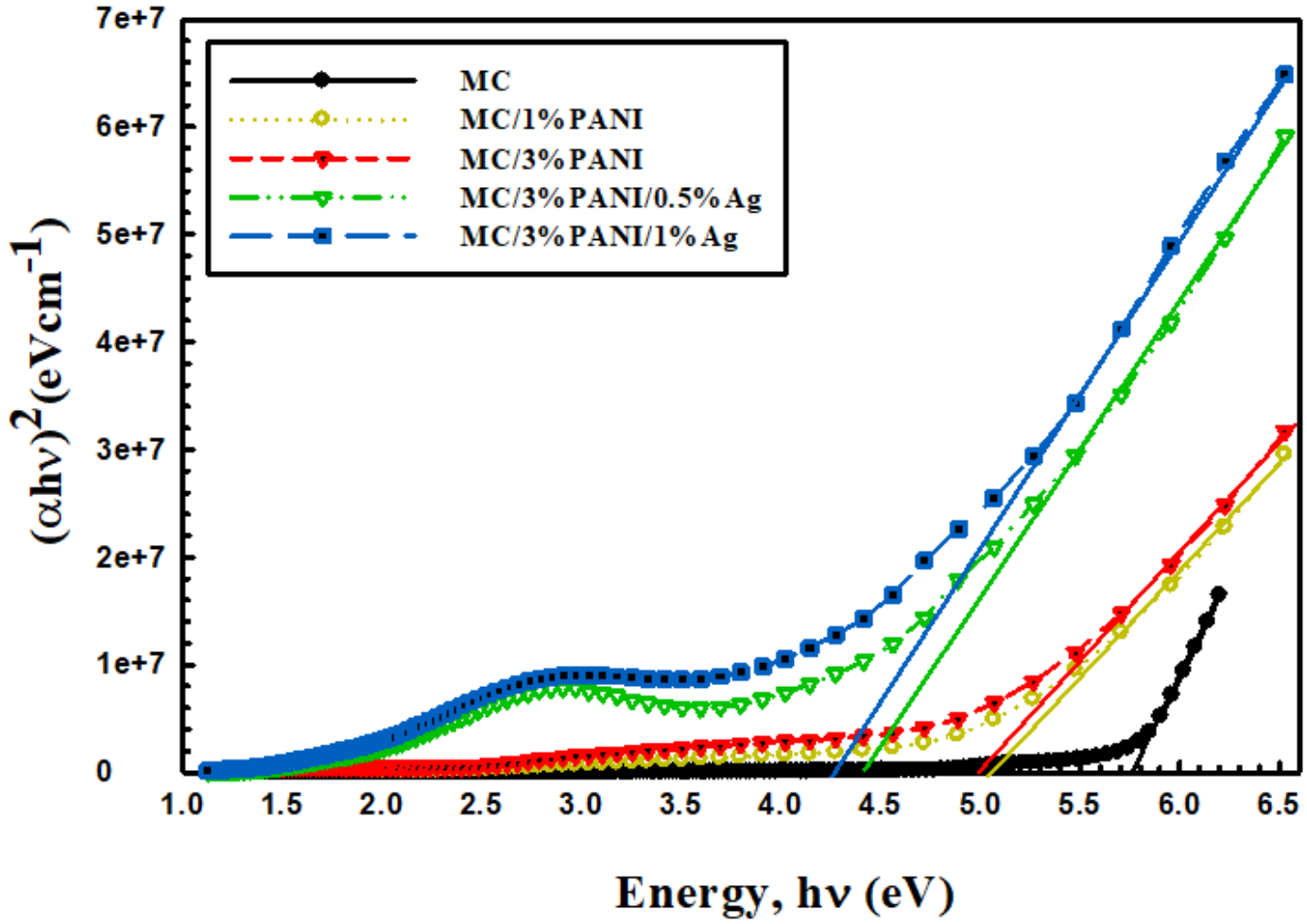

Figure 5

The relation between (αhν)2 against photon energy (hν) for pristine MC, MC/1%PANI, MC/3%PANI, MC/3%PANI/0.5%Ag and MC/3%PANI/1%Ag films.

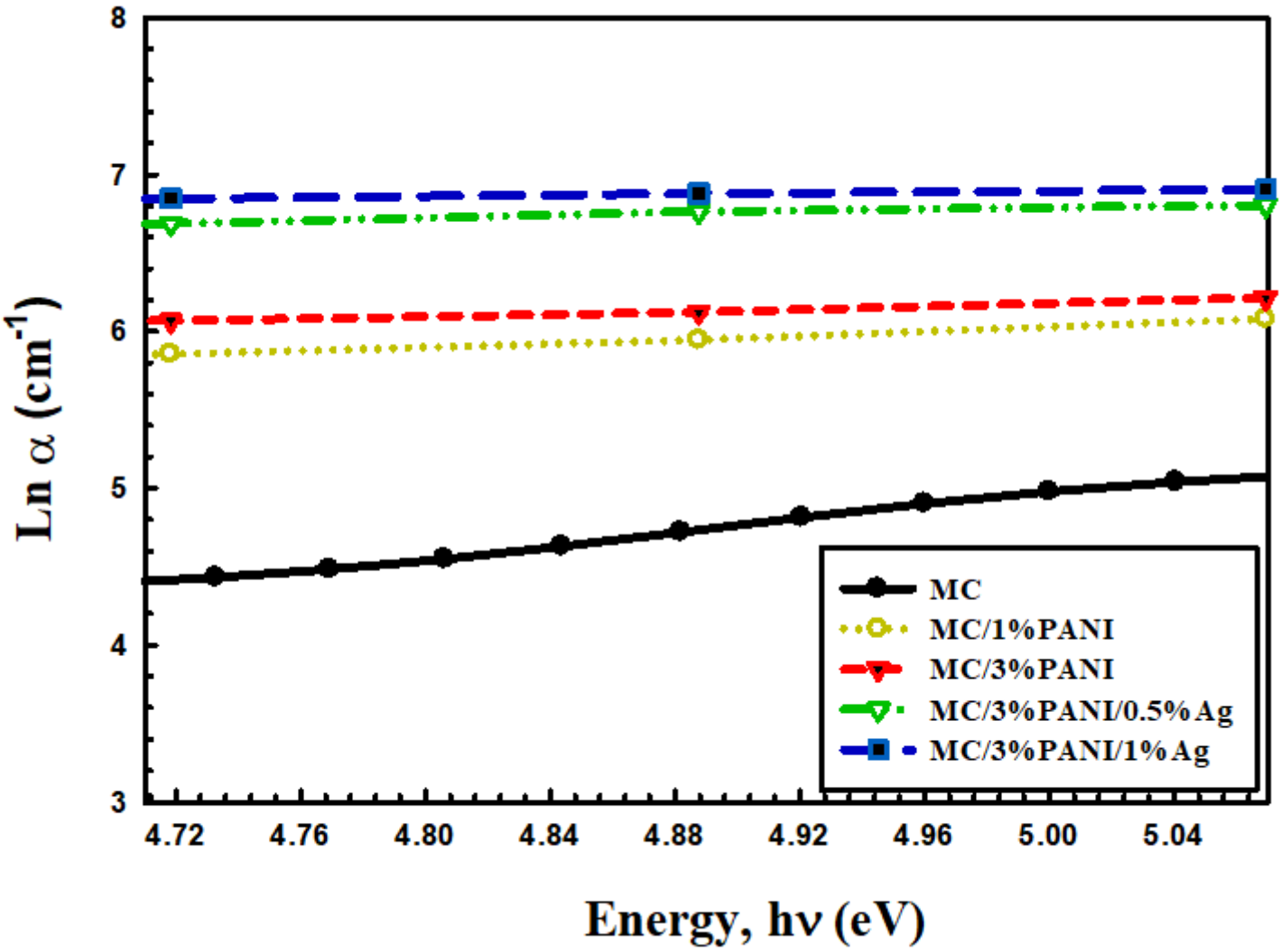

Figure 6

Absorption coefficient versus photon energy for pristine MC, MC/1%PANI, MC/3%PANI, MC/3%PANI/0.5Ag and MC/3%PANI/1%Ag films

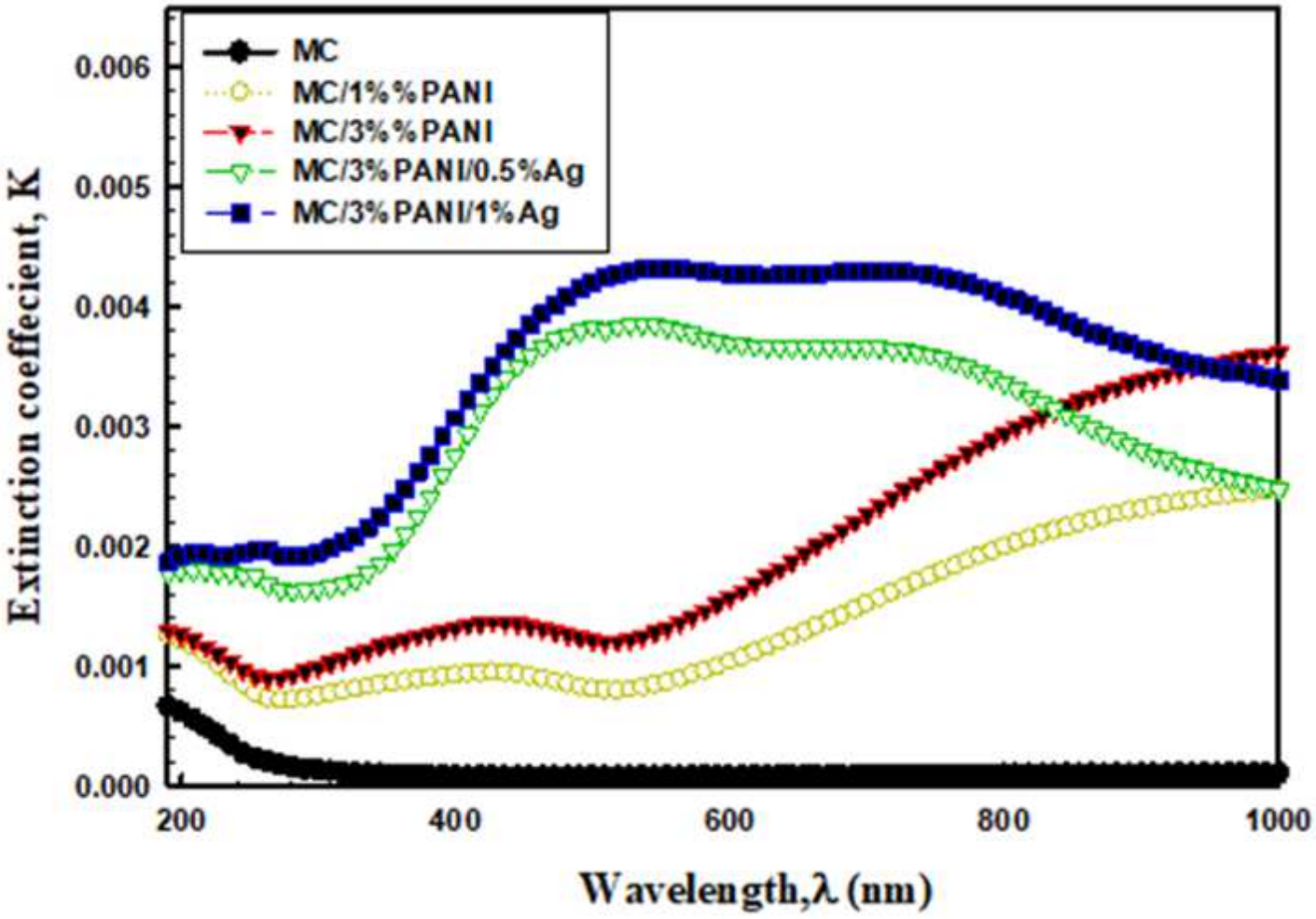

Figure 7

The extinction coefficient k versus wavelength λ for pristine MC, MC/1%PANI. MC/3%PANI, MC/3%PANI/0.5%Ag and MC/3%PANI/1%Ag films.

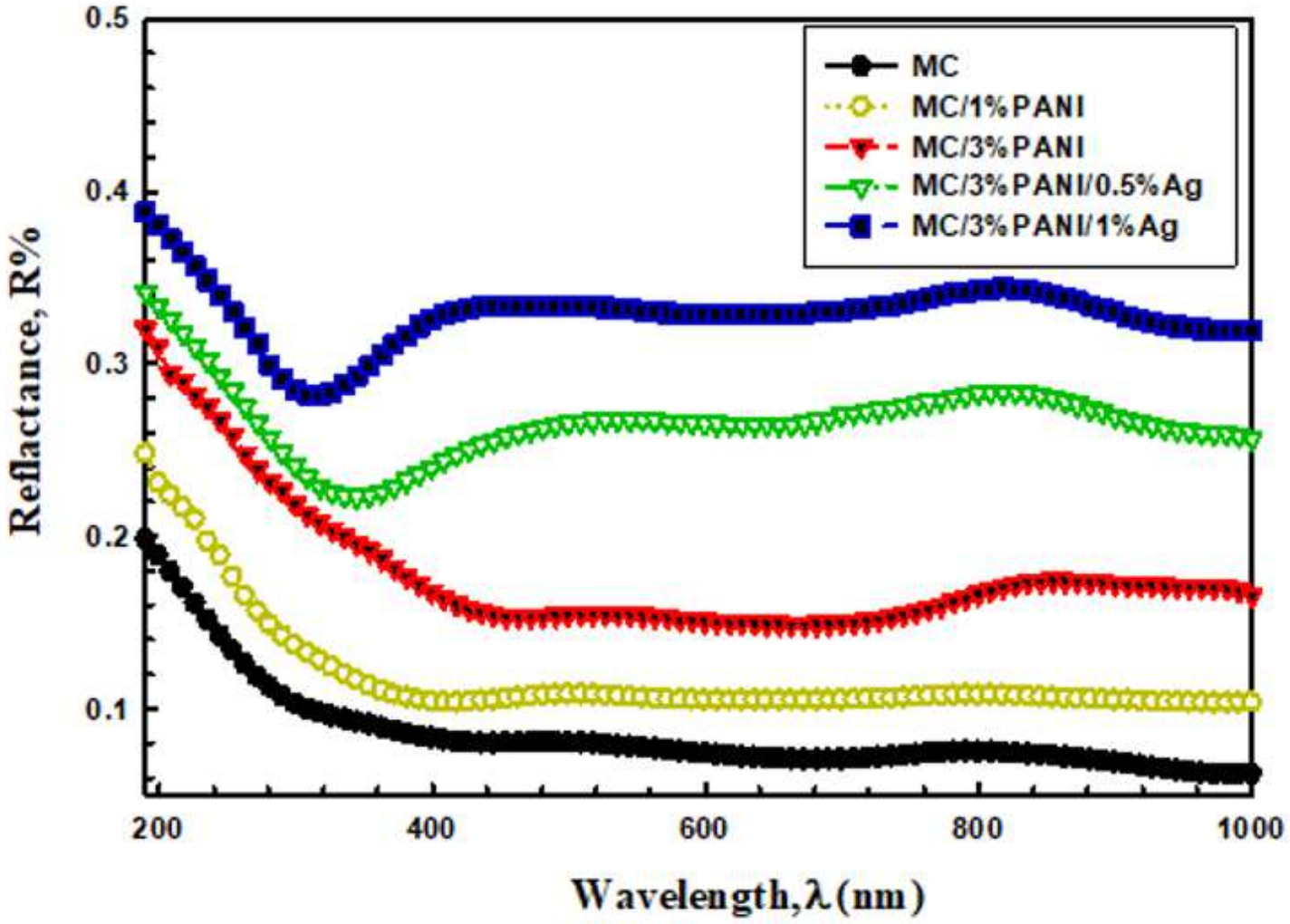

Figure 8

The reflectance (R) as a function of wavelength (λ) for pristine MC, MC/1%PANI, MC/3%PANI, MC/3%PANI/0.5%Ag and MC/3%PANI/1%Ag films.

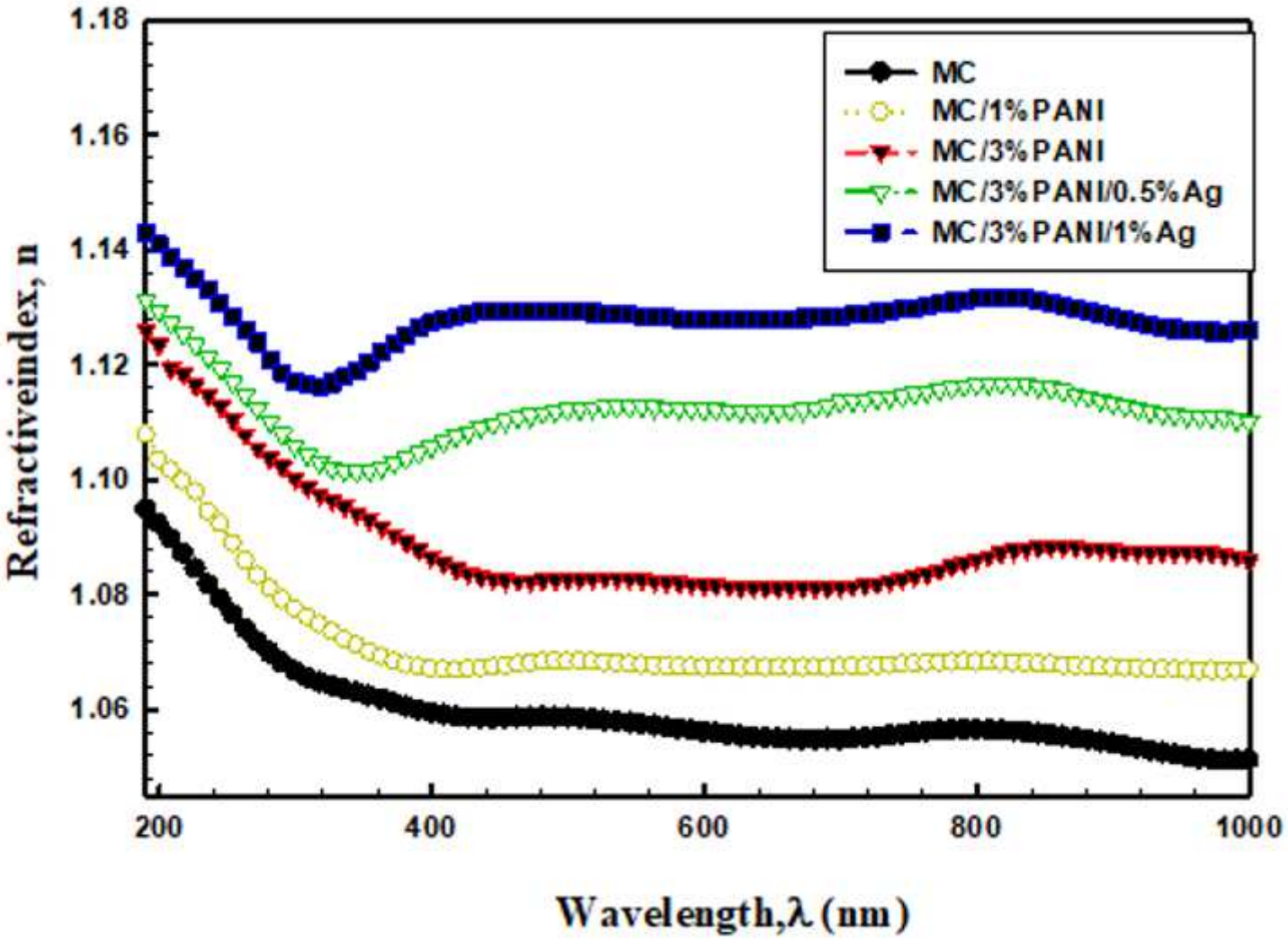

Figure 9

The refractive index n versus wavelength λ of pristine MC, MC/1%PANI, MC/3%PANI, MC/3%PANI/0.5%Ag and MC/3%PANI/1%Ag films.

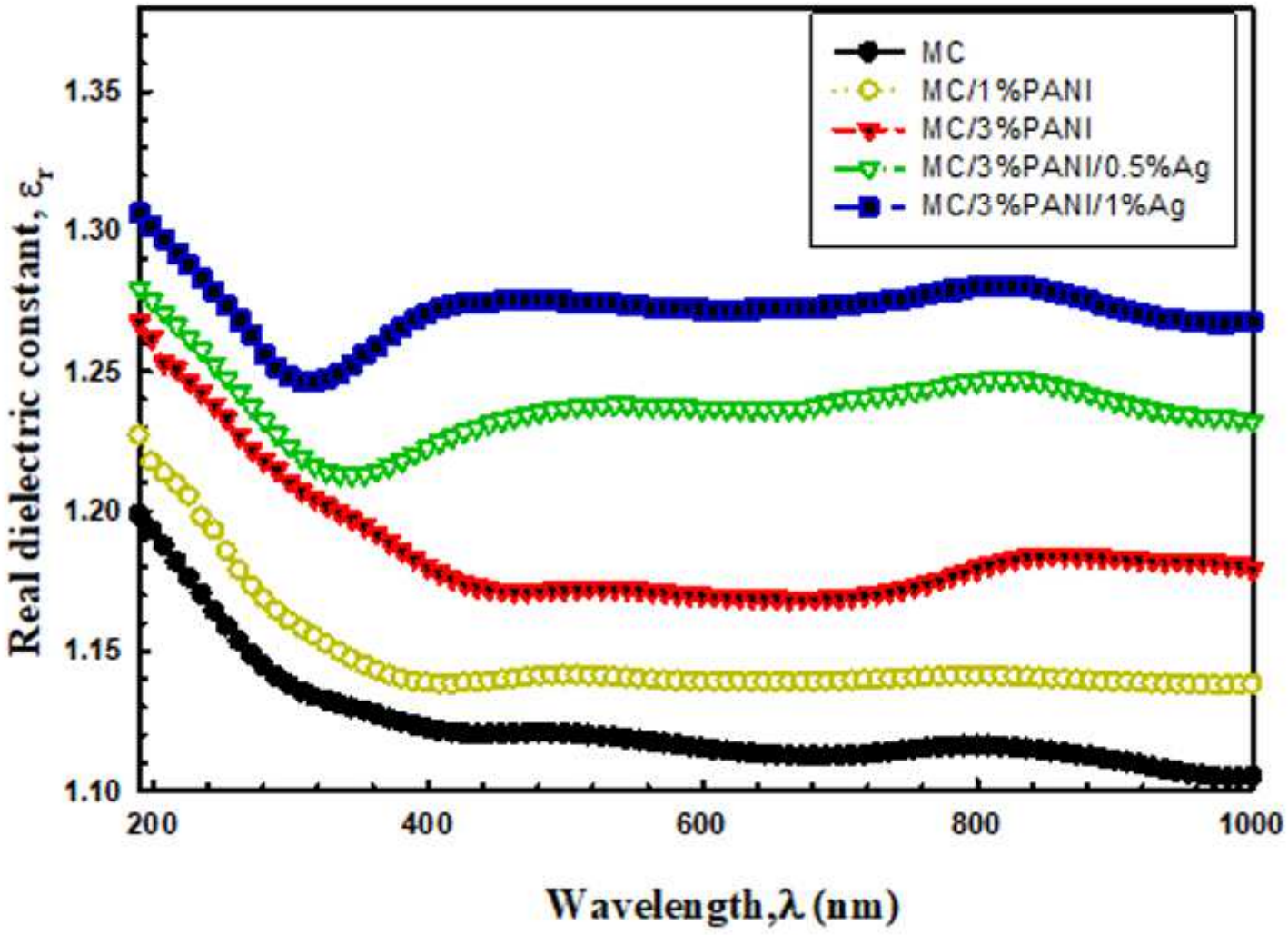

Figure 10

Variation of real dielectric constant εr, as a function of wavelength λ of pristine MC, MC/1%PANI, MC/3%PANI, MC/3%PANI/0.5%Ag and MC/3%PANI/1%Ag films.

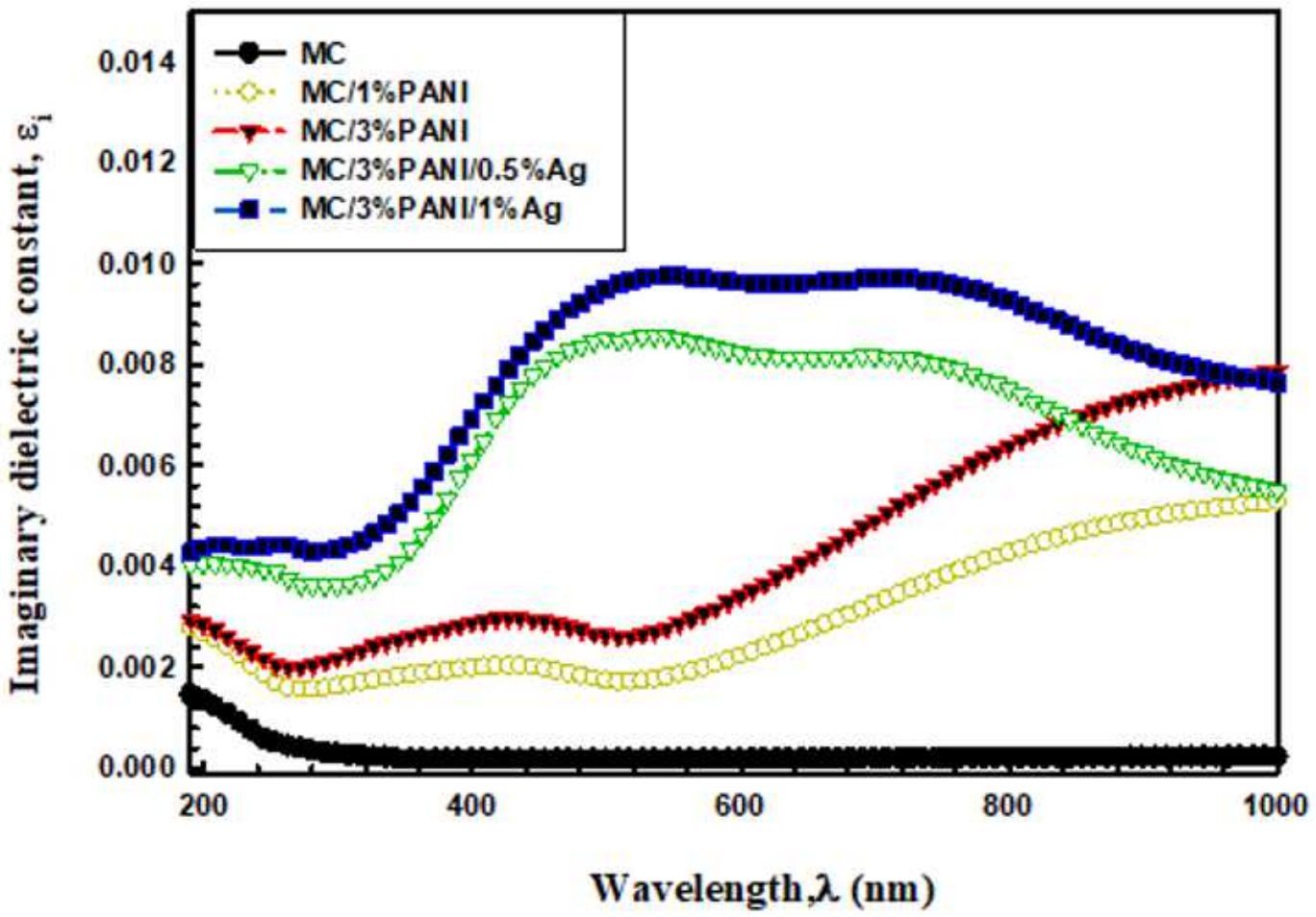

Figure 11

Imaginary dielectric constant (εi), as a function of photon energy (hv) for pristine MC, MC/1%PANI, MC/3%PANI, MC/3%PANI/0.5%Ag and MC/3%PANI/1%Ag films.

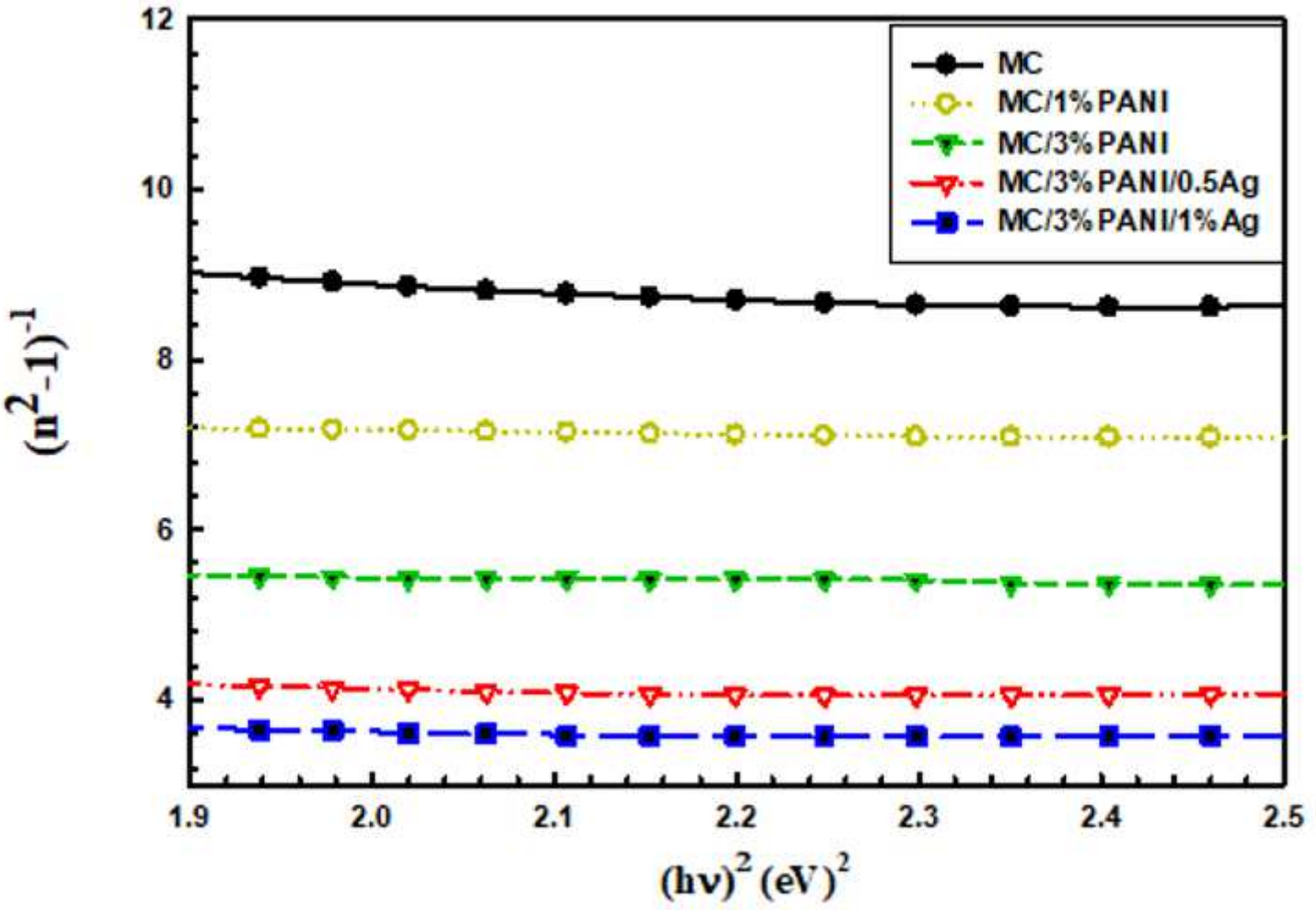

Figure 12

The relation between (n2-1)-1 and (hυ)2 for pristine MC, MC/1%PANI, MC/3%PANI, MC/3%PANI/0.5%Ag and MC/3%PANI/1%Ag films.

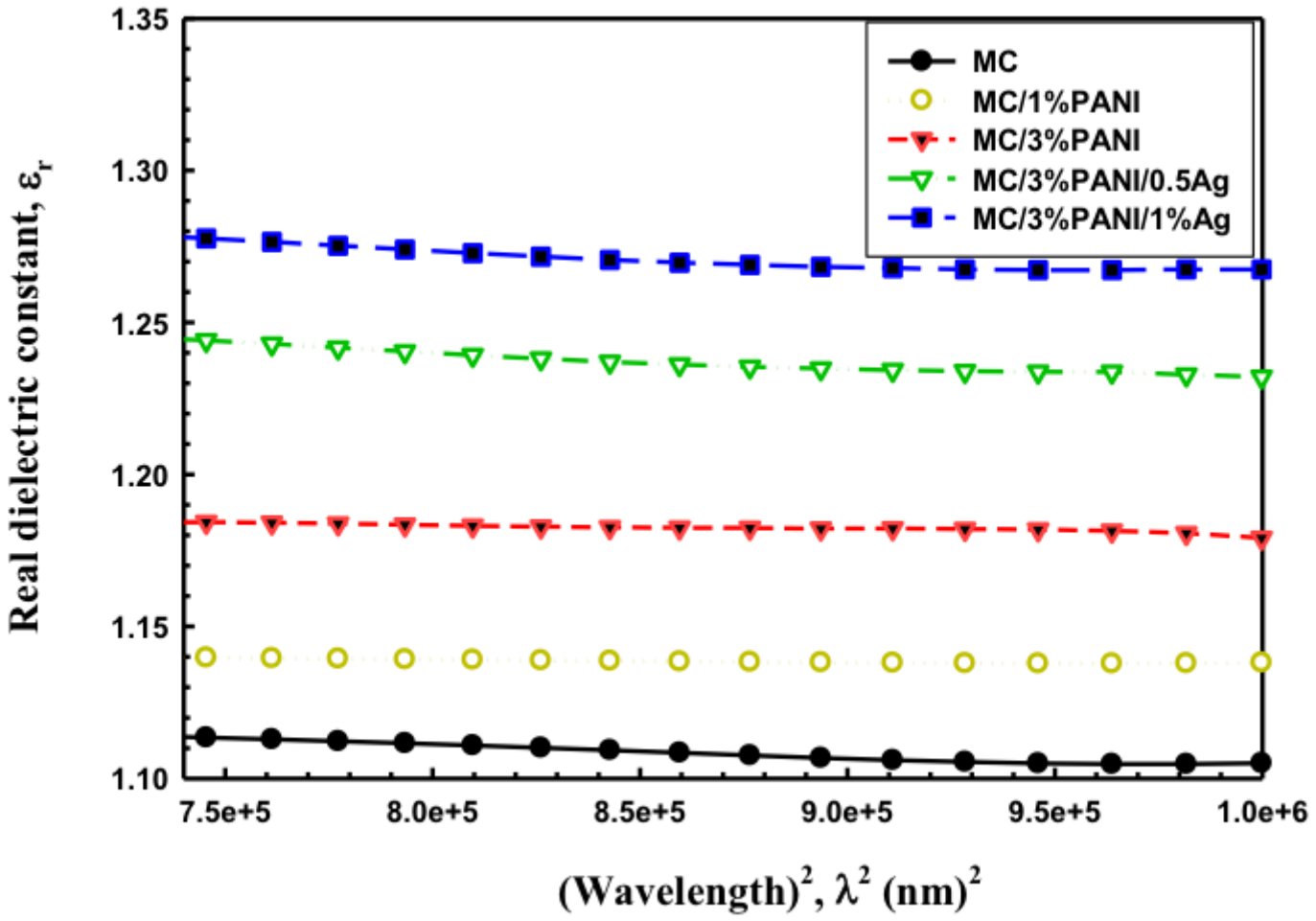

Figure 13

Variation of real dielectric constant (εr), as a function of wavelength (λ2) for pristine MC, MC/1%PANI, MC/3%PANI, MC/3%PANI/0.5%Ag and MC/3%PANI/1%Ag films.

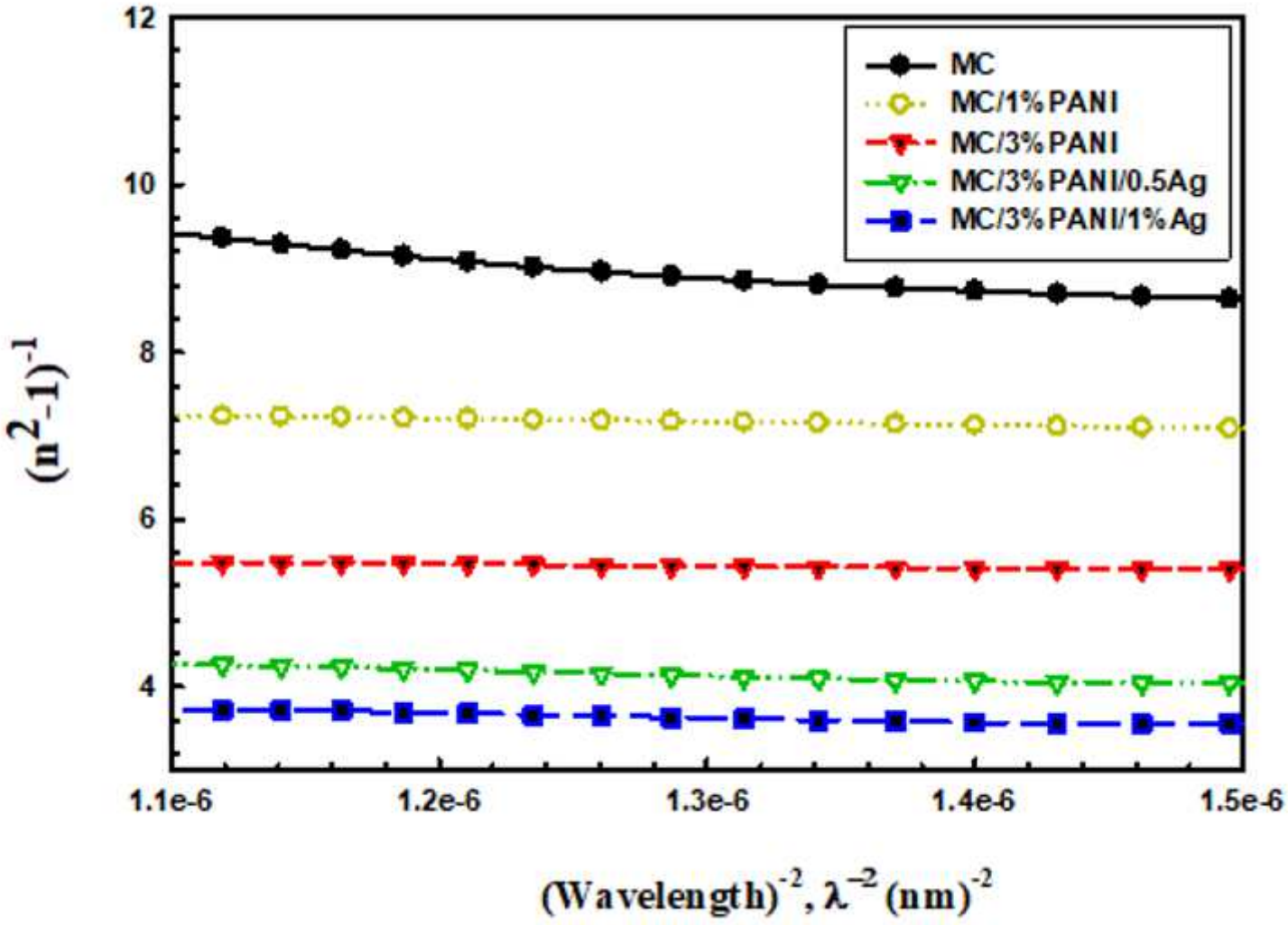

Figure 14

The relation between (n2-1)-1 and (λ)-2 for pristine MC, MC/1%PANI, MC/3%PANI, MC/3%PANI/0.5%Ag and MC/3%PANI/1%Ag films.

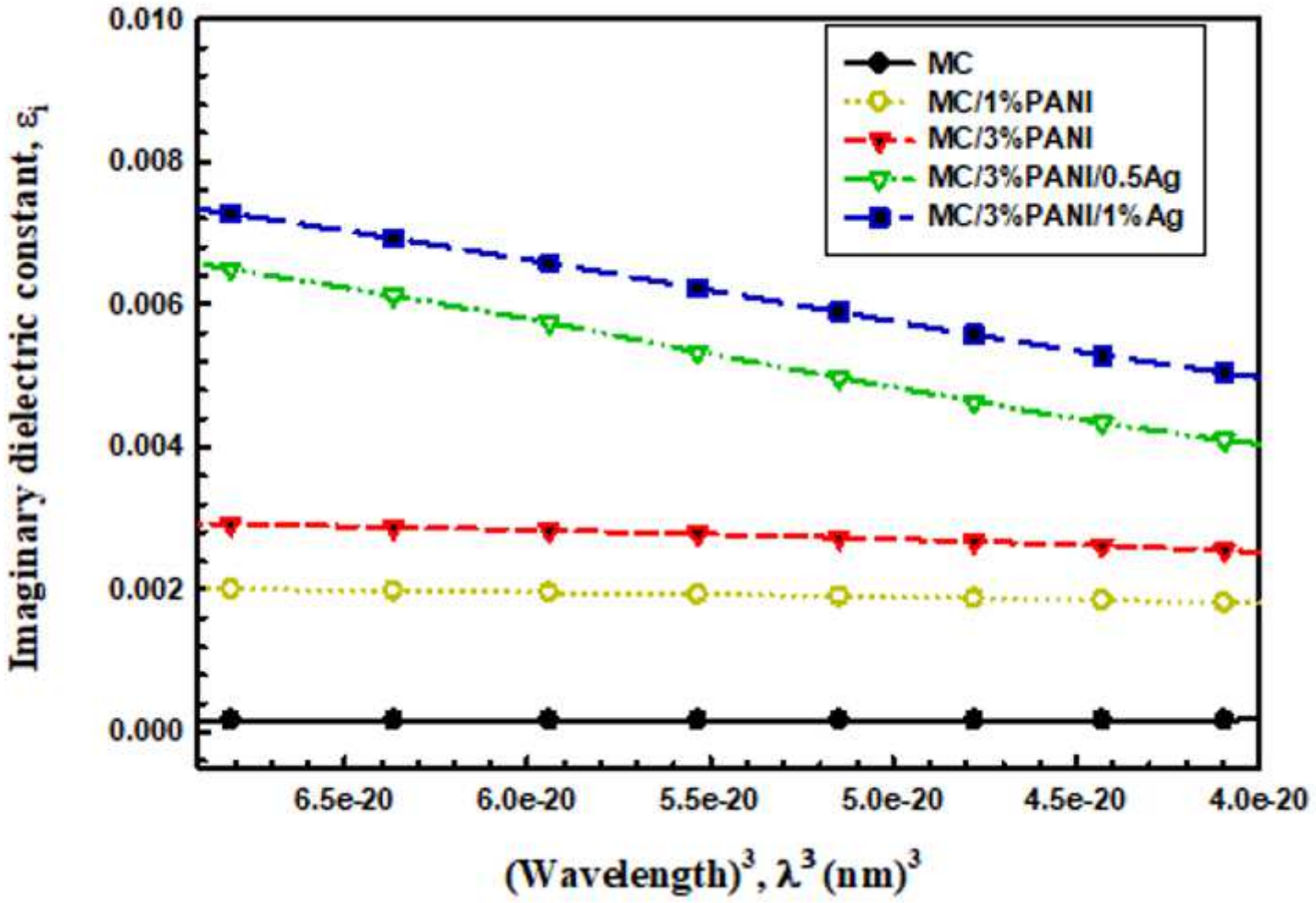

Figure 15

Relation between imaginary dielectric constant εi and λ3 for pristine MC, MC/1%PANI, MC/3%PANI, MC/3%PANI/0.5%Ag and MC/3%PANI/1%Ag films.

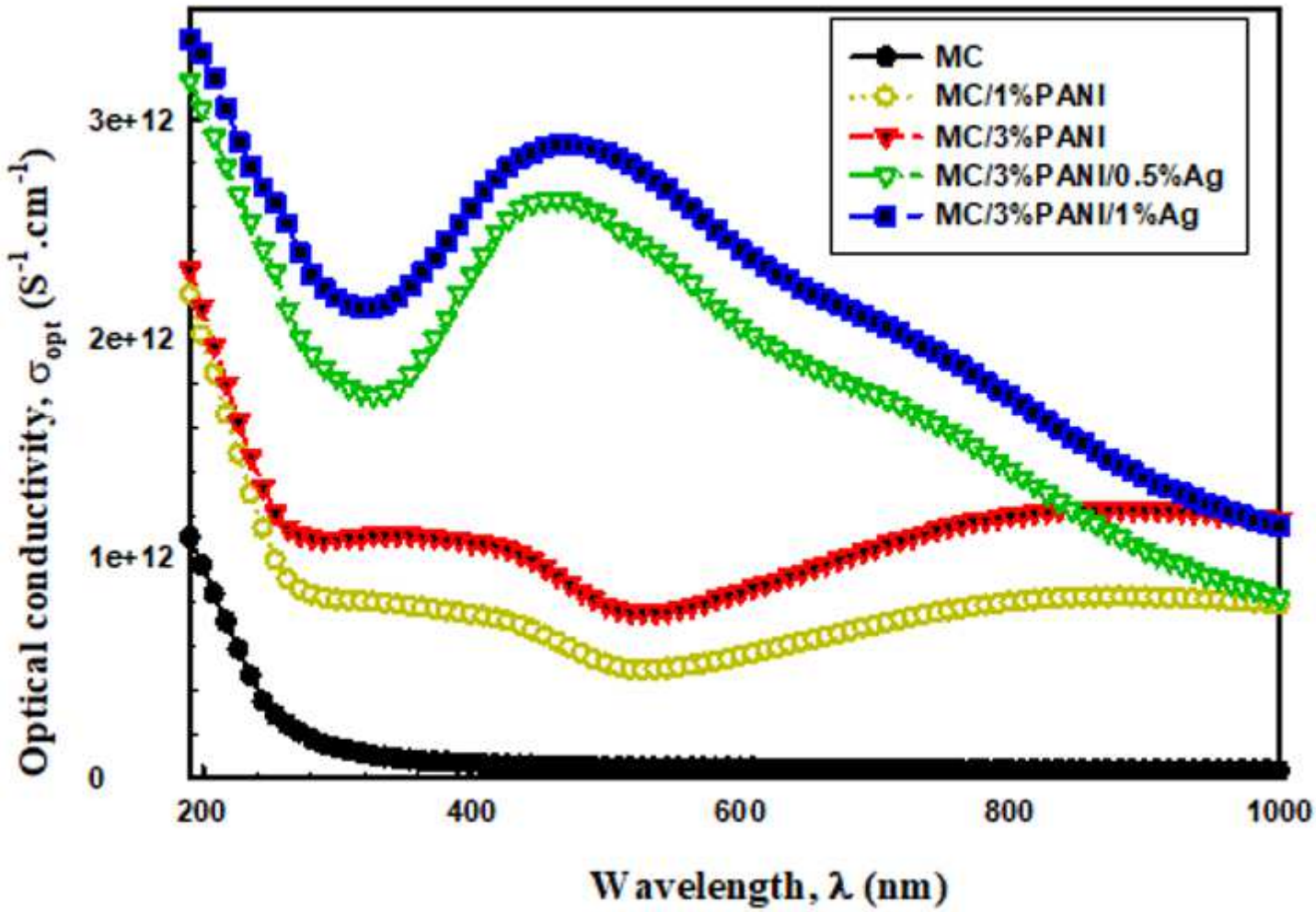

Figure 16

Variation of optical conductivity with photon energy for pristine MC, MC/1%PANI, MC/3%PANI, MC/3%PANI/0.5AgNPs and MC/3%PANI/1AgNPs films.

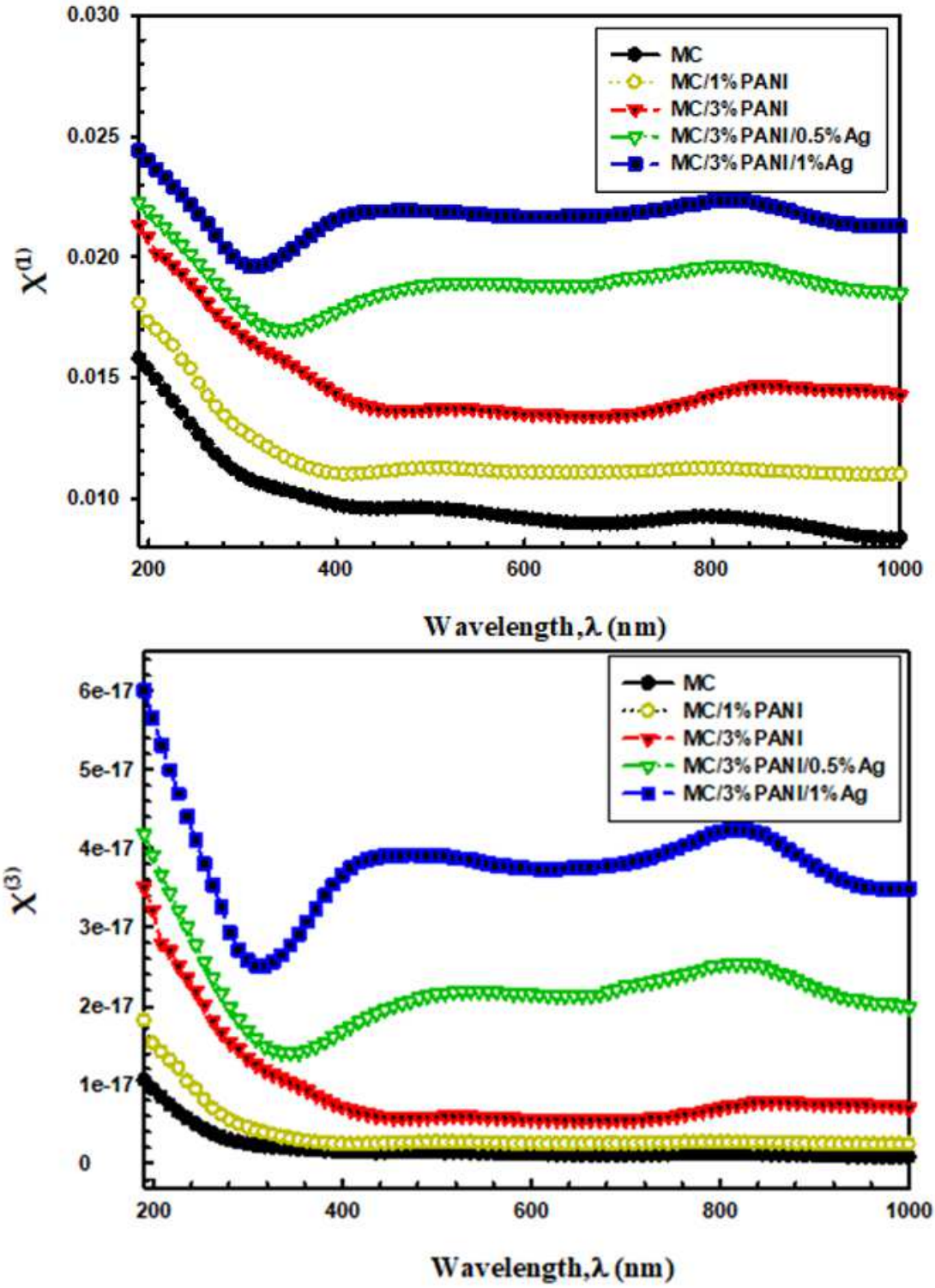

Figure 17

(a). Linear optical susceptibilityX^((1)) and (b) Non-linear optical susceptibility X^((3)) as a function of wavelength (λ) of pristine MC, MC/1%PANI, MC/3%PANI, MC/3%PANI/0.5%Ag and MC/3%PANI/1%Ag films.

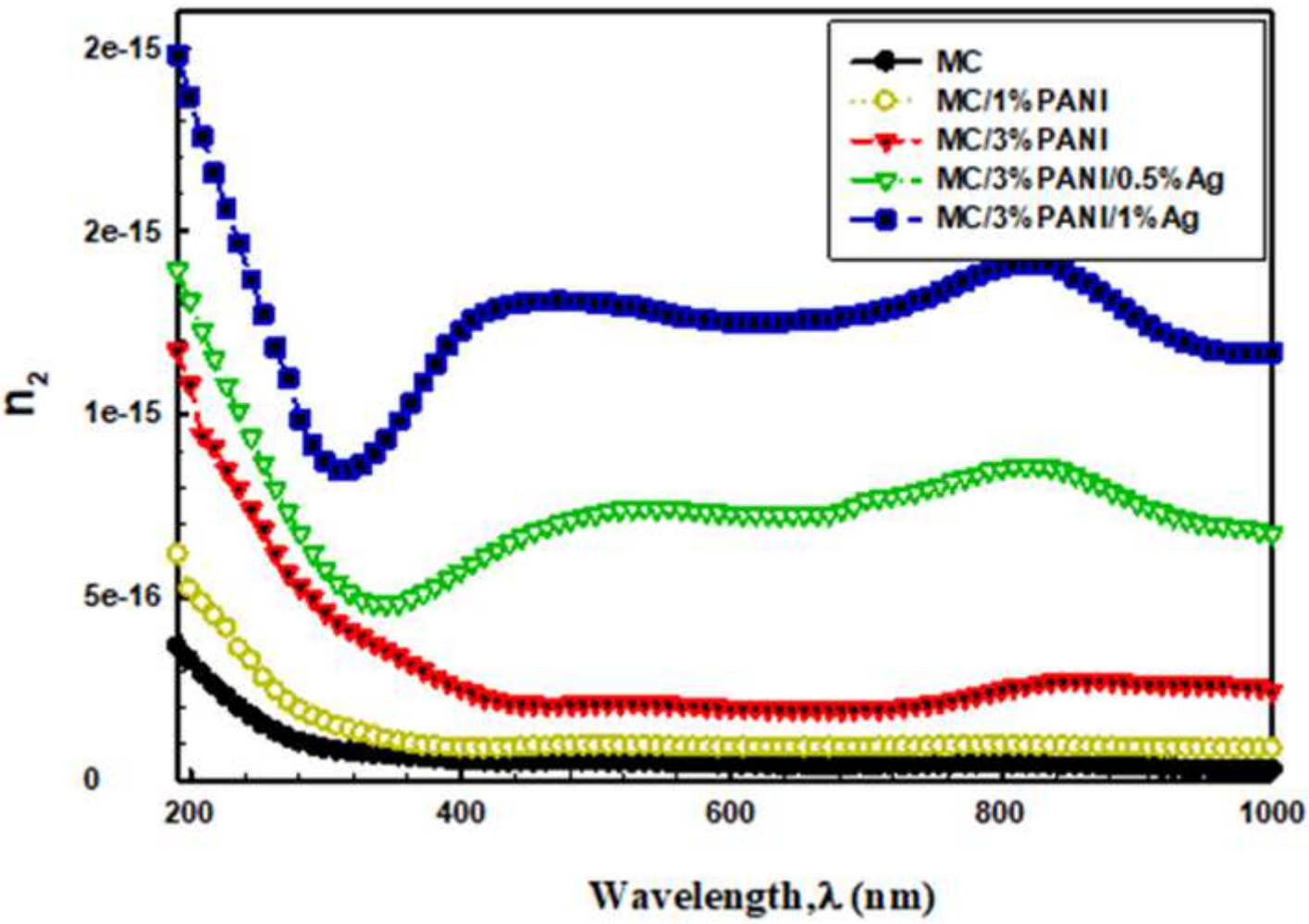

Figure 18

Non-linear refractive index (n2) as a function of wavelength (λ) of pristine MC, MC/1%PANI, MC/3%PANI, MC/3%PANI/0.5%Ag and MC/3%PANI/1%Ag films.